LANGMUIR Article
Cite This: Langmuir 2019, 35, 16185−16200
pubs.acs.org/Langmuir

# Structural and Chemical Evolution of L-Cysteine Nanofilm on Si(111)-$\sqrt{3}\times\sqrt{3}$-Ag: From Preferential Growth at Step Edges and Antiphase Boundaries at Room Temperature to Adsorbate-Mediated Metal Cluster Formation at Elevated Temperature

Hanieh Farkhondeh, Fatemeh R. Rahsepar,† Lei Zhang, and Kam Tong Leung*

WATLab and Department of Chemistry, University of Waterloo, Waterloo, Ontario N2L3G1, Canada

Supporting Information

**ABSTRACT:** The interaction of cysteine molecules with the Si(111)-$\sqrt{3}\times\sqrt{3}$-Ag surface has been investigated over the submonolayer to multilayer regime using X-ray photoelectron spectroscopy, scanning tunneling microscopy, and density functional theory calculations. With both upper step and lower step terraces, step edges, and antiphase boundaries, the $\sqrt{3}\times\sqrt{3}$-Ag overlayer supported on Si(111) provides a rich two-dimensional template for studying site-specific biomolecular interactions. As an amino acid with three functional groups, cysteine is found to chemisorb through S−H bond cleavage and S−Ag bond linkage first at step edges and antiphase boundaries followed by island formation and expanded growth onto terraces. Intermolecular interactions are dominated by zwitterionic hydrogen bonding at higher coverages, producing a porous unordered interfacial layer composed of cysteine agglomerates at room temperature. Upon annealing, cysteine adsorbates induce structural transformation of the uniform $\sqrt{3}\times\sqrt{3}$-Ag reconstructed surface lattice into metallic Ag clusters with a narrow size distribution and short-range ordering. Preferential nanoaggregate formation of cysteine at defect sites and cysteine-induced metal cluster formation promise a new approach to fabricating nanoclusters for potential applications in chemical sensing and catalysis.

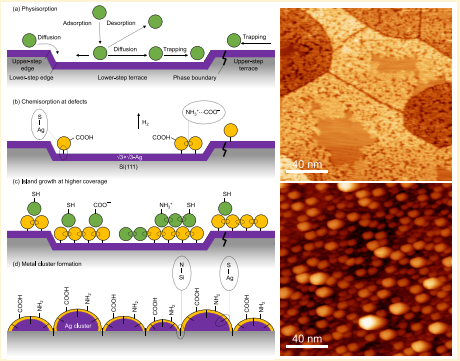


## INTRODUCTION

The study of physical and chemical phenomena occurring at the interface between organic molecules and a solid surface has attracted much interest due to their wide range of applications in optics, electronics, biotechnology, and nanoscience. Understanding such interfacial interactions at the molecular level is pivotal to the design and development of emerging devices such as hybrid organic−semiconductor devices, biological and chemical sensors, and catalysts. There have been numerous studies on the interface between an organic adlayer and a metal or semiconductor substrate. Metal surfaces are interesting because they offer a two-dimensional electron gas system to effect weak physical interactions with organic molecules. On the other hand, semiconductor surfaces such as Si(111)7×7 contain reactive dangling bonds that make possible directional covalent bonding with organic molecules. Semiconductor surfaces are therefore great candidates for organic functionalization in bio- or chemical sensing and nanoelectronics applications. Hybrid metal−semiconductor surfaces are another class of solid surfaces that have attracted a lot of recent attention due to the provision of the structural and electronic properties from both metal and semiconductor surfaces and to the potential creation of synergetic properties.

The Si(111)-$\sqrt{3}\times\sqrt{3}$-Ag surface has been one of the most studied hybrid surfaces by various surface-sensitive techniques. One technical significance of this type of substrate is that a usually well-ordered, two-dimensional, single-atom thick metal overlayer is supported on the Si(111) substrate, making it readily customizable for applications in molecular devices appropriate for large-scale integration and other thin-film fabrication protocols. It has also been historically one of the most important prototypes for the metal/semiconductor interfaces, because of the interesting physics revealed in its atomic arrangements, surface electronic states, and electronic transport phenomena.[1] A silver-passivated silicon surface is obtained by depositing one monolayer of Ag atoms on the Si(111)7×7 substrate, thereby terminating all of the dangling bonds perfectly and making the surface inert. Upon annealing to the appropriate temperature, the surface is composed of ordered Si and Ag trimers in an alternating island (upper terrace) and hole (lower terrace) pair arrangement. The resulting atomic structure of the Si(111)-$\sqrt{3}\times\sqrt{3}$-Ag surface is best described by honeycomb-chained triangle and inequivalent triangle structures, which are closely related to each other such that the former is a fully symmetrical version of the latter.[2−8] The Ag atoms are arranged on the top layer with a 3-fold rotational symmetry, and the Ag−Si bonding in the honeycomb-chained triangle configuration has been

Received: September 10, 2019
Revised: October 23, 2019
Published: October 29, 2019






DOI: 10.1021/acs.langmuir.9b02852
Langmuir 2019, 35, 16185−16200

reported to be heteropolar in character, with considerable charge transfer from the Ag adlayer to the Si substrate.[9] The most abundant surface defects of Si(111)-$\sqrt{3}\times\sqrt{3}$-Ag include the step edges and antiphase boundaries. A step edge is the transitional interface between the upper terrace and the lower terrace (shown in a schematic model in Figure S1), while an antiphase boundary is the phase boundary between terraces of the same height.

A number of studies have focused on the adsorption of large $\pi$-conjugated organic molecules on the Si(111)-$\sqrt{3}\times\sqrt{3}$-Ag surface for organic thin film applications, which include 3,4,9,10-perylene tetracarboxylic dianhydride (PTCDA),[10] 3,4,9,10-perylene tetracarboxylic diimide (PTCDI),[11] thiophene,[12−14] metal phthalocyanine,[15] metal porphyrines,[16,17] $C_{60}$,[18] and pentacene,[19] as well as of smaller molecules such as trimesic acid,[20] terephthalic acid,[21] and adenine,[22] at both low temperature and room temperature. All of these molecules adsorb in a flat configuration via weak molecular coupling with the surface, as realized by physisorption through the interaction of their $\pi$-conjugated rings with the two-dimensional electron gas of the surface. The focus of these physisorption studies has been the nature of self-assembly into molecular structures. To date, there is only one study on chemisorption of organic molecules on Si(111)-$\sqrt{3}\times\sqrt{3}$-Ag in which thiol-modified ferrocene molecules are reported to undergo S−H dissociation and chemisorption via S−Ag linkage preferentially on defect sites and occasionally on terrace sites at room temperature.[23] Chemisorption is arguably a more important alternative mechanism for immobilizing molecules, allowing robust modification of the electronic properties of Si-based surfaces and development of stable devices with organic molecules to enable operation at a more desirable temperature such as room temperature.

The objective of the present study is 2-fold: (1) to understand the interactions between the Si(111)-$\sqrt{3}\times\sqrt{3}$-Ag surface and a prototypical amino acid with multiple functional groups, such as cysteine ($C_\beta OOHC_\alpha HNH_2C_\gamma H_2SH$), at room temperature and at elevated temperature and (2) to investigate any potential synergetic properties of the Si(111)-$\sqrt{3}\times\sqrt{3}$-Ag surface functionalized with these S-containing amino acid molecules for potential applications. As the building blocks of proteins, amino acids represent one of the most important classes of small organic molecules. They are also of special interest to the engineering of biomimetic materials because their different functional groups (carboxylic acid group, amino group, and thiol group in the case of cysteine) could link to one another and to the surface, making them ideal molecular systems for studying various types (and their combinations) of long-range and short-range interactions. Understanding these important interactions will enable efficient construction and manipulation of their supramolecular architectures on metal surfaces crucial for the performance of bioanalytical devices and biocompatible materials.[24−34] Among the 20 naturally occurring amino acids, cysteine is the only "biogenic" amino acid that contains a thiol side chain. Cysteine is known to be a strong ligand for transition metals, making it a potential candidate as a chemical receptor for metal ions. It is also widely used not only for anchoring larger biomolecules to metal nanoparticles in bioanalytical and drug delivery protocols but also for molecular electronics development by taking advantage of its dissociated thiol group (thiolate) to produce strong covalent bonding with noble metals. A variety of ordered structures of cysteine has been obtained on different metal surfaces of Cu,[35−37] Ag,[38−41] and Au[37,39,42−58] through both physisorption and chemisorption at various temperatures as characterized by scanning tunneling microscopy (STM), X-ray photoelectron spectroscopy (XPS), and quantum mechanical calculations based on density functional theory (DFT).

Previous experimental and theoretical studies of our group have shown that cysteine adsorbs on Si(111)7×7 in the initial growth stage through dehydrogenation of the thiol and amino groups and formation of both S−Si and N−Si (unidentate and bidentate) covalent bonding. This is followed by lateral and vertical intermolecular hydrogen bonding at the interfacial and transitional layers for low cysteine exposures and by zwitterionic interactions for thicker layers.[59] Here, we report a comprehensive approach to determine the chemical nature of L-cysteine adsorption on the Si(111)-$\sqrt{3}\times\sqrt{3}$-Ag surface and their pertaining implications for surface functionalization. Our combined STM and XPS measurements, complemented by large-scale DFT calculations, reveal a clear bonding picture of interfacial layer formation and film growth of cysteine at and above room temperature. Our XPS data show that cysteine chemisorbs on the surface through S−H bond cleavage and S−Ag anchorage, while zwitterionic interactions dominate even at lower coverages. Our STM results depict preferential nucleation of cysteine adspecies near step edges and their growth into disordered coral-reef shaped islands on the terraces of the Si(111)-$\sqrt{3}\times\sqrt{3}$-Ag surface. Our DFT calculations confirm cysteine chemisorption through S−Ag linkage and further determine the most favorable adsorption configurations involving single and multiple molecules on the surface. We also identify the processes occurring at the interface between the molecules and the substrate from the early growth stage to the multilayer regime at room temperature as well as the structural and chemical evolution of cysteine on Si(111)-$\sqrt{3}\times\sqrt{3}$-Ag upon annealing to elevated temperatures. Of particular interest is our first observation of adspecies-induced formation of Ag clusters above 175 °C.

## EXPERIMENTAL AND COMPUTATIONAL DETAILS

The experiments were carried out in a custom-designed multichamber ultrahigh vacuum (UHV) system (Omicron Nanotechnology, Inc.) operated at a background pressure of $5\times10^{-11}$ mbar. The analysis chamber was equipped with an XPS spectrometer (consisting of a SPHERA analyzer, a seven-channel detector, and a monochromatic Al K$\alpha$ source) and a variable-temperature scanning tunneling microscope. An atomically sharp, chemically etched W wire was used as the STM tip to probe the surface in a constant current mode. With the tip grounded, all images were obtained with a tunneling current of 0.2 nA and a sample bias of −2 and +2 V for filled-state and empty-state imaging, respectively. The metal and organic vapor depositions were performed with the respective high-temperature and low-temperature organic effusion cells (Dr. Ebert, MBE-Komponenten GmbH) in two separate UHV chambers. The substrate was a single-side polished, n-type Si(111) chip (11×2 $mm^2$, 0.3 mm thick) with a resistivity of 5 mΩ cm (Virginia Semiconductor, Inc.). An atomically clean Si(111)7×7 surface was prepared by flash annealing at 1200 °C after the Si substrate was thoroughly degassed by direct-current heating at 400 °C for 12 h. Silver was deposited onto the Si substrate for 120 s followed by direct-current annealing to 500 °C for 120 s.[60] The cleanliness of the Si(111)-$\sqrt{3}\times\sqrt{3}$-Ag surface was then validated by STM, XPS, and low-energy electron diffraction (LEED) before deposition of cysteine.

Cysteine (99.5% purity, Fluka) was exposed to the Si(111)-$\sqrt{3}\times\sqrt{3}$-Ag surface by increasing the effusion cell temperature to 130 °C. During deposition, the background pressure of the chamber was



DOI: 10.1021/acs.langmuir.9b02852
Langmuir 2019, 35, 16185−16200

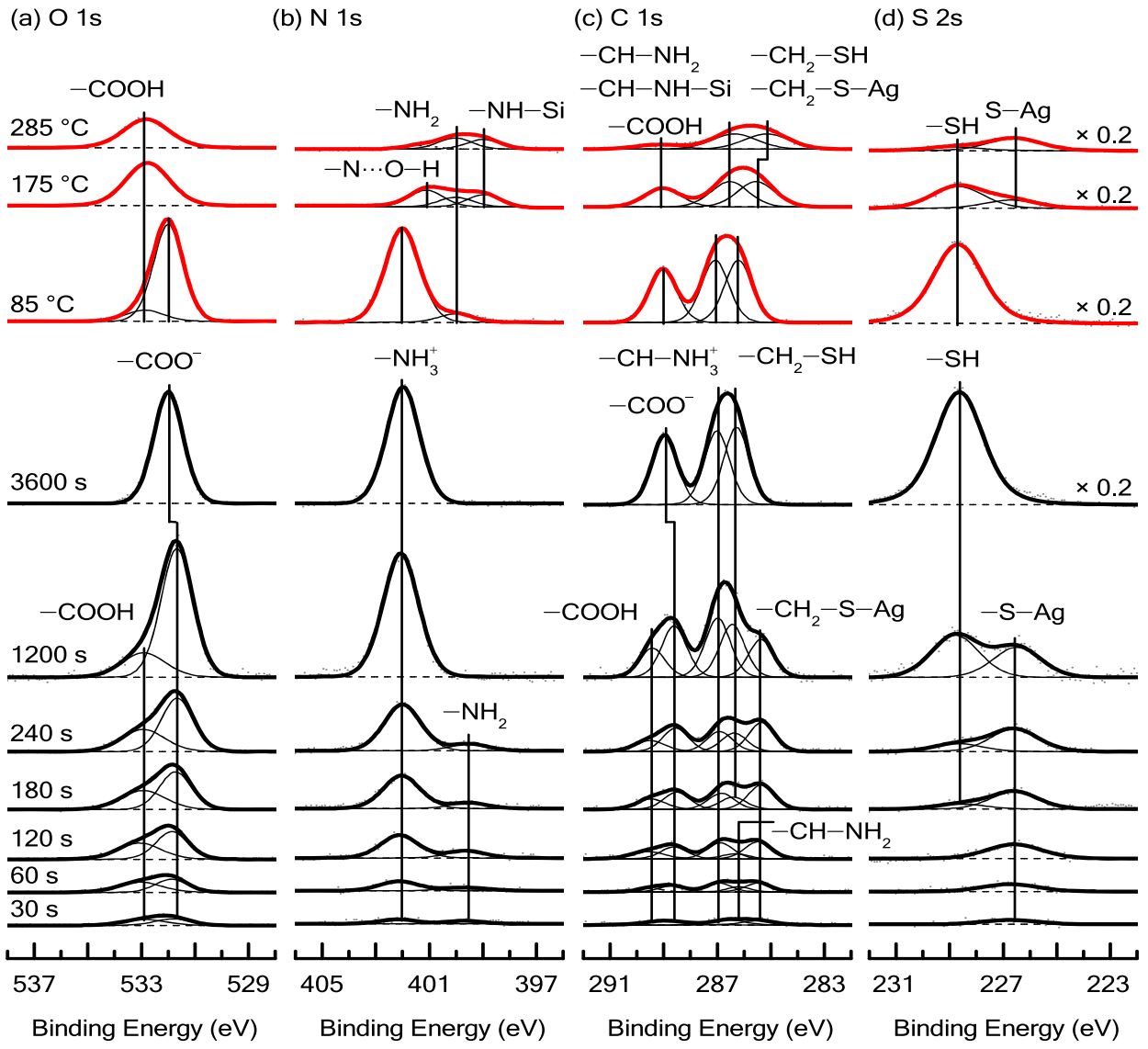


**Figure 1.** Evolution of O 1s, N 1s, C 1s, and S 2s XPS spectra of cysteine deposited on Si(111)-$\sqrt{3}\times\sqrt{3}$-Ag as a function of exposure time (30−3600 s) and of the as-grown cysteine multilayer film (obtained with a 3600 s exposure) upon annealing to 85, 175, and 285 °C.

$2\times10^{-9}$ mbar. To confirm the purity of the cysteine powder, the cracking pattern was monitored in situ using a quadrupole mass spectrometer (Stanford Research Systems RGA-300) and was found to be in good accord with the literature.[61] To obtain submonolayer to multilayer films, cysteine was evaporated onto the Si(111)-$\sqrt{3}\times\sqrt{3}$-Ag surface at room temperature with different exposure times. Each exposure was performed on a freshly prepared Si(111)-$\sqrt{3}\times\sqrt{3}$-Ag surface. For the surface covered with a thick cysteine film, the sample was annealed sequentially to 85, 175, and 285 °C, each for 600 s, using resistive heating. The sample was then allowed to cool back to room temperature after each annealing step before characterization. All of the STM and XPS experiments were conducted with the sample held at room temperature. The XPS spectra were recorded at a pass energy of 20 eV with an energy resolution of 0.7 eV full width at half-maximum (fwhm) for the Ag $3d_{5/2}$ photoline at 368.3 eV. Using the Casa XPS software, Gaussian−Lorentzian line shapes were employed to fit the spectra after appropriate correction with the Shirley background.

Ab-initio DFT calculations that included the long-range dispersion correlation and van der Waals interactions (DFT-D2) were employed to obtain the equilibrium geometries of plausible adsorption structures of L-cysteine on flat terraces (and step edges) of a model surface consisting of a 4×4 slab of Si(111)-$\sqrt{3}\times\sqrt{3}$-Ag unit cells (with a total of 16 $\sqrt{3}\times\sqrt{3}$-Ag unit cells). The first-principle total energy calculations were performed within the projector augmented wave (PAW) potentials and the generalized gradient approximation (GGA) based on the Perdew−Burke−Ernzerhof (PBE) exchange-correlation functional. The Vienna Ab-initio Simulation Package (VASP, version 5.4) with the MedeA platform (Materials Design, version 2.19) was used. The plane wave expansion cutoff energy was set to 400 eV, and the surface Brillouin zone was sampled at the Γ point with a *k*-point spacing of 0.5 $Å^{-1}$. The structures of all stationary points were obtained with the conjugate-gradient algorithm. All Si and Ag atoms were relaxed until the forces on all atoms were less than 0.05 eV/Å, while the energy threshold defining self-consistency of the electron density was set to $10^{-5}$ eV, with the Methfessel−Paxton smearing of 0.2 eV. In this study, we used an optimized structure of the honeycomb-chained triangle model for the Si(111)-$\sqrt{3}\times\sqrt{3}$-Ag substrate in which each unit cell contained three Ag atoms (in the topmost layer) and three Si atoms underneath. A periodic 4×4 slab with 16 1×1 unit cells of Si(111)-$\sqrt{3}\times\sqrt{3}$-Ag was used as the model surface. This slab consisted of a topmost layer of Ag trimers (48 Ag atoms) bonded to a layer of Si trimers underneath and three underlying Si bilayers (336 Si atoms in total) as well as a vacuum gap



DOI: 10.1021/acs.langmuir.9b02852
*Langmuir* 2019, 35, 16185−16200

of 10 Å. The bottom layer of Si atoms in the slab was terminated with 48 H atoms. An adsorbate cysteine molecule (or, where appropriate, a thiolated cysteine adspecies) was placed on the topmost layer of the slab to simulate covalent bonding to Ag or Si adatoms in the interfacial layer. For the fully relaxed geometry calculations, the positions of the H atoms were fixed while those of the Si and Ag atoms were relaxed.

## RESULTS AND DISCUSSION

**Thiol Dissociative Adsorption of Cysteine and Growth of Supported Cysteine Film at Room Temperature.** In addition to the carboxylic acid and amino groups common in the 20 proteinogenic amino acids, cysteine is one of two sulfur-containing amino acids and it is the only amino acid that contains a thiol group. Cysteine is found in its neutral form in the gas phase, while it exists in its zwitterionic form with a protonated amino group and a deprotonated carboxylic acid group in both aqueous solution and solid state.[62] To analyze the evolution and stability of chemical states of cysteine during nanofilm growth, we conduct XPS measurements on films obtained with low to high cysteine exposures at room temperature and on the as-grown multilayer film at elevated temperatures. Figure 1 shows the XPS spectra of the O 1s, N 1s, C 1s, and S 2s regions of cysteine on the Si(111)-$\sqrt{3}\times\sqrt{3}$-Ag surface as a function of exposure time. It should be noted that since the S 2p peak at 164.0 eV partially overlaps with the broad Si plasmon peak near 168.0 eV, we have chosen the S 2s peak to monitor the change in the S chemical-state composition in the present work. To compare our results of the interface adsorption with the bulk, we use the cysteine multilayer grown on the Si(111)-$\sqrt{3}\times\sqrt{3}$-Ag surface after the 3600 s exposure, for which the peak positions closely resemble those observed for the cysteine multilayer film on Si(111)7×7 and for the cysteine powder in the solid phase.[59] In the multilayer regime (3600 s exposure in Figure 1), we find that the S 2s peak appears predominantly at 228.6 eV, indicating the presence of an intact thiol group. The single O 1s peak at 532.0 eV and the N 1s peak at 402.0 eV correspond to, respectively, the deprotonated carboxylic acid group ($-COO^-$) and protonated amino group ($-NH_3^+$) in the zwitterions. The C 1s signal can be fitted with three main components at 286.3, 287.0, and 289.0 eV corresponding to the alkyl carbon atoms in C−SH and C−$NH_3^+$ moieties and to the carboxylate group, respectively.

In the low-exposure regime of 30−120 s, the S 2s spectra show only one peak at 226.6 eV, which is 2.0 eV lower in binding energy than the multilayer thiol peak. This feature is clearly related to the chemisorption of cysteine through the dehydrogenated thiol group. In our previous study on the adsorption of cysteine on Si(111)7×7,[59] we found the S 2s feature of the S−Si bond to be located at 227.4 eV. The lower binding energy by 0.8 eV for the observed S 2s feature therefore indicates S−Ag rather than S−Si linkage.[63] In the N 1s region, two well-defined peaks are observed at 399.5 and 402.0 eV, with the former being less intense than the latter. The N 1s peak at 402.0 eV is consistent with the protonated amino group in the zwitterionic adspecies. The position of deprotonated amino (and N−Si linkage) has been reported to downshift by 3.2 eV with respect to the protonated amino group, while the intact amino group is known to be located at 1.8 eV lower than the position of zwitterionic N 1s feature.[46,59] Since the separation between the two N 1s features in our current results is 2.5 eV, the peak at the lower binding energy can be attributed to the intact amino group that is likely closer to the surface to enable its interaction with the surface Ag atoms through its lone-pair electrons. The presence of the deprotonated amino group, however, cannot be ruled out, because given that the NH−Si feature has been observed for the adsorption of cysteine on Si(111)7×7, the presence of the NH−Si linkage on Si-rich defect sites is plausible and should be expected. The interaction of the intact amino group through its lone-pair electrons has also been reported for cysteine adsorption on the Ag(111) surface.[38] The sharper O 1s feature at 531.7 eV (fwhm = 1.4 eV) agrees well with the deprotonated carboxylic acid group position, while the broader O 1s peak at 532.9 eV (fwhm = 1.9 eV) can be attributed to the carbonyl oxygen and hydroxyl oxygen atoms in the carboxylic acid group. The presence of two well-defined neutral and zwitterionic features in the N 1s and O 1s regions along with the single thiolate feature in the S 2s region indicate the presence of two types of cysteine adspecies on the surface at the same time. The neutral adspecies could represent single cysteine molecules bonded to the surface through their dehydrogenated thiol group in an upright configuration or in a nearly flat configuration with the amino and carboxylic acid functional groups leaning toward the surface. The latter configuration is expected to be viable at very low coverages due to the absence of neighboring molecules, where the individually adsorbed molecules have enough space to exert their interactions with the surface through all of their available free functional groups. On the other hand, the presence of the zwitterionic species suggests the formation of small clusters (or islands) of two or more cysteine molecules with zwitterionic intermolecular interactions between the protonated amino group and the deprotonated carboxylic acid group while chemically bonded to the surface through the dehydrogenated thiol group. The peak maxima and the peak assignments of the fitted peaks for individual components are given in Table S1, and their relative intensities are shown in Figure S2.

Further increasing the exposure time to 180 s leads to the emergence of a second peak in the S 2s region at 228.6 eV corresponding to an intact thiol group. Both the thiol (at 228.6 eV) and the thiolate features (at 226.6 eV) further develop with increasing exposure time until the thiol feature becomes dominant at 1200 s. Concurrently, the N 1s and O 1s peaks grow in intensity with the zwitterionic features becoming more prominent. This can be attributed to the growth of the existing chemisorbed cysteine islands and to increased nondissociative adsorption of cysteine molecules simultaneously, both of which involve zwitterionic intermolecular coupling. Our companion STM study of Si(111)-$\sqrt{3}\times\sqrt{3}$-Ag before (i.e., pristine surface) and after cysteine exposure (results discussed below) shows that for exposures up to 240 s the coverage of cysteine adspecies appears to be less than one monolayer, where we define one monolayer as a fully covered Si(111)-$\sqrt{3}\times\sqrt{3}$-Ag surface in the STM image. Physisorption of incoming cysteine species could occur directly on both the uncovered terraces of the Si(111)-$\sqrt{3}\times\sqrt{3}$-Ag surface and the existing cysteine islands. Using the adsorbate-induced attenuation of the Si 2p signal and the calculated electron mean free path in a uniformly thick organic film,[64] we estimate the thickness of the organic layer for the 1200 s exposure to be 1.1 nm. The S 2s spectrum for the 1200 s exposure (Figure 1d) consists of 42% thiolate species and 58% thiol species. As the thickness of a chemisorbed molecular layer (1 ML) is estimated to be 0.51 nm (discussed further in our DFT



DOI: 10.1021/acs.langmuir.9b02852
Langmuir 2019, 35, 16185−16200

study below), the relative intensity of the thiolate S 2s feature therefore indicates an approximate coverage of 0.86 ML of chemisorbed species in the interfacial layer. Since the amount of thiol species in the S 2s region is higher than the chemisorbed ones, the rest of the interfacial layer is composed of adspecies on top of the interfacial layer bound not directly to the surface but to one another through zwitterionic interlayer interactions or weak van der Waals forces. Using the relative intensities of the thiolate feature in the other S 2s spectra (Figure S2) and the calculated thicknesses of their films, we estimate the cysteine layer coverage for each exposure time. Accordingly, the weakly bound species (with the thiol feature) start to appear at the 180 s exposure, where the coverage is estimated to consist of 0.36 ML of chemisorbed species adsorbed directly on the surface and 0.16 ML of weakly bound species on the top side of the interface layer. Similarly, the coverage of the chemisorbed species for the 240 s exposure is calculated to be 0.47 ML, while that for the weakly bound species both on the top side of the interfacial layer and in the second adlayer is estimated to be 0.29 ML.

Interestingly, while the intensity change of the N 1s feature attributed to the amino group (at 399.5 eV) generally follows an increasing trend with increasing exposure time, it is less discernible than the trend observed for the S 2s features (Figure S2). The minor fluctuation in the intensity change with increasing exposure supports our hypothesis that this feature is connected to preferential adsorption on surface defect and other non-terrace sites. As a freshly Si(111)-$\sqrt{3}\times\sqrt{3}$-Ag surface is prepared for each cysteine exposure, each preparation could lead to a slightly different amount of surface defects and a different extent of terrace sizes. The lack of a well-defined trend with increasing exposure found for this N 1s feature for the amino group therefore supports adsorption on defect and non-terrace sites. At the 1200 s exposure, since the estimated thickness of the molecular adlayer (1.1 nm) remains less than the photoelectron escape depth (~9.0 nm), the S 2s features in the interfacial layer remain easily detectable. However, the $-NH_2$ feature related to the interfacial layer is not present anymore, suggesting that the $-NH_2$ moieties that are not involved in the zwitterionic interactions have most likely been protonated with additional H atoms originating from breakage of the S−H bonds. The increase in the O 1s intensity for the carboxyl component (−COOH) up to the 1200 s exposure can also be explained in a similar way.[38] At lower coverages, on the other hand, the presence of the −COOH component is related to either the isolated cysteine molecules adsorbed on surface defects or the free −COOH groups at the outer region of the cysteine islands.

The corresponding C 1s spectra for the 30−120 s exposures consist of two broad bands with three peaks at lower binding energies of 285.3, 286.1, and 286.7 eV and two peaks at higher binding energies of 288.4 and 289.3 eV, which can be attributed to $-CH_2-S-Ag$, $-CH_2-NH_2$, and $-CH_2-NH_3^+$ and to $-COO^-$ and COOH moieties, respectively.[38] For higher exposures of 180−1200 s, a new peak at 286.3 eV corresponding to the $-CH_2-SH$ moiety (with an intact thiol group) in the zwitterionic layer[38,59] is observed. The growth of this feature appears to overtake the intensity of the nearby $-CH_2-NH_2$ feature (at 286.1 eV). At the 3600 s exposure, the S 2s feature of the $-CH_2-SH$ component at 228.6 eV, along with the C 1s features for the $-CH_2-NH_3^+$ component at 287.0 eV and the $-COO^-$ component at 289.0 eV, have become the predominant features, consistent with the emergence of a zwitterionic film.

**Silver Nanocluster Formation at Elevated Temperature.** Our observation of the zwitterionic intermolecular interactions in the cysteine multilayer film on Si(111)-$\sqrt{3}\times\sqrt{3}$-Ag is consistent with the adsorption of a cysteine zwitterionic film found on other noble metal single-crystal surfaces, including Ag(111), Au(111), and Au(110), at submonolayer and monolayer coverages.[38,46,65−67] To further understand the nature of the interactions of cysteine with the Si(111)-$\sqrt{3}\times\sqrt{3}$-Ag surface and to investigate the stability of the supported cysteine multilayer film, thermal treatment is performed on a supported multilayer film obtained with a 3600 s cysteine exposure (Figure 1). The top three spectra shown in Figure 1 correspond to the spectral evolution of the as-grown cysteine film obtained with a 3600 s exposure upon sequential annealing to 85, 175, and 285 °C for 600 s each (followed by cool down back to room temperature before the XPS measurement). Annealing at 85 °C appears to cause discernible intensity reduction for the zwitterionic features and reappearance of the minor −COOH O 1s and $-NH_2$ N 1s features, which could be due to partial desorption of the film, thereby exposing free amino and carboxylic acid groups. The peak positions and widths of the predominant features remain unchanged with respect to the as-deposited multilayer zwitterionic film. Further annealing to 175 °C has led to desorption of ~80% of the original film, as shown by the significant intensity reduction found in the thiol S 2s feature. Furthermore, the thiolate S 2s feature of the interfacial layer has re-emerged at 226.6 eV (Figure 1d). The O 1s spectrum shows a single broader feature at 532.5 eV, which corresponds to the carboxylic acid group. On the other hand, the N 1s spectrum can be fitted with three new features at 399.1, 400.1, and 401.1 eV, which can be assigned to −NH−Si, $-NH_2$, and N···O−H (or N···S−H) moieties, respectively.[59] The C 1s spectrum is found to consist of two broad bands. The lower binding energy band can be fitted with two components corresponding to S-containing moieties such as $-CH_2-S-Ag$ and $-CH_2-SH$ (at 285.5 eV) and to N-containing moieties such as −C−NH−Si and $-C-NH_2$ (at 286.5 eV), while the higher binding energy band at 289.0 eV corresponds to the −COOH feature.

In the study of cysteine adsorption on Si(111)7×7, we conclude that the cysteine zwitterionic structure could exist up to 85 °C, while the transitional layer (second adlayer) consisting of interlayer hydrogen bonds are stable even after annealing to 175 °C.[59,68] In the present work, no transitional layer is observed and physisorption is found to occur at the second adlayer on the as-formed chemisorbed layer. However, after annealing, the chemical composition of the cysteine film on Si(111)-$\sqrt{3}\times\sqrt{3}$-Ag appears to resemble that of cysteine on Si(111)7×7, which suggests the presence of a transitional layer on the interfacial layer. We propose the following mechanism for the formation of the transitional layer. Upon annealing the cysteine film on Si(111)-$\sqrt{3}\times\sqrt{3}$-Ag, the interfacial layer undergoes a structural and chemical change during annealing and desorption of the thick zwitterionic film, which results in disruption of the zwitterionic intermolecular interactions (in the first adlayer). Through their free amino and carboxylic acid groups, the cysteine molecules in the disrupted interfacial layer could interact vertically with the second layer leading to the formation of interlayer H bonds. This in effect results in the formation of the transitional layer



DOI: 10.1021/acs.langmuir.9b02852
Langmuir 2019, 35, 16185−16200

between the newly formed H-bonded layer and the zwitterionic layer on top. This process may also propagate to the third or higher adlayer, depending on the original thickness of the zwitterionic film and the heating and desorption rates of the film. Our proposed mechanism is supported by the presence of both −COOH and $-NH_2$ features and the corresponding $-COO^-$ and $-NH_3^+$ (H-bond related) features in the O 1s and N 1s regions. Formation of H-bonded groups has also been observed in the transitional layer of a cysteine film on Si(111)7×7.[68]

Upon annealing to 285 °C, the −COOH C 1s feature (at 289.0 eV) has been reduced in intensity discernibly more than the N- and S-related C 1s peaks, indicating the decomposition of the cysteine film. However, the positions of the −NH−Si (Figure 1b) and −S−Ag peaks (Figure 1d) remain unchanged, suggesting the presence of intact chemisorbed (thiolated) cysteine or its decomposition fragments. This is consistent with the decomposition of cysteine powder over the temperature range of 185−280 °C.[69] The presence of atomic S (and S-containing fragments) has also been reported for thermal evolution of thiophene adsorbed on Si(100) and Pt(111) and for cysteine adsorption on Si(111)7×7 upon annealing at 285 °C.[59,70,71]

To investigate the influence of cysteine adsorption and thermal treatment on the $\sqrt{3}\times\sqrt{3}$-Ag overlayer itself, we show in Figure 2 the corresponding XPS spectra of the Ag 3d region for the Si(111)-$\sqrt{3}\times\sqrt{3}$-Ag surface before and after the exposure of cysteine for 1200 and 3600 s and upon annealing of the as-grown 3600 s cysteine multilayer film on the surface.

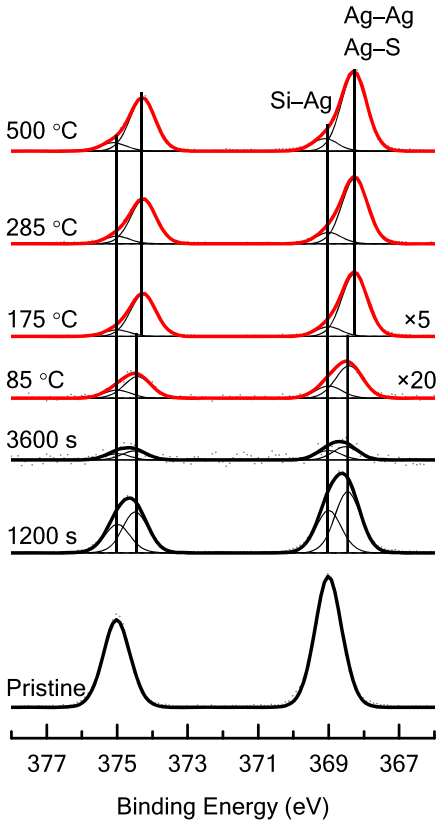


**Figure 2.** XPS spectra of the Ag 3d region for a pristine Si(111)-$\sqrt{3}\times\sqrt{3}$-Ag surface before and after cysteine exposure for 1200 and 3600 s, and for the resulting as-grown (3600 s) multilayer film upon annealing to 85, 175, 285, and 500 °C.

The pristine Si(111)-$\sqrt{3}\times\sqrt{3}$-Ag surface exhibits a sharp Ag $3d_{5/2}$ (Ag $3d_{3/2}$) feature at 369.0 eV (375.0 eV, fwhm = 0.85 eV), which corresponds to the Si−Ag bonds in the Ag trimers of the $\sqrt{3}\times\sqrt{3}$ surface template. Cysteine exposure for 1200 s results in the broadening of the overall Ag 3d band, which can be fitted with two Ag $3d_{5/2}$ (Ag $3d_{3/2}$) peaks with nearly the same widths at 369.0 (375.0 eV) and 368.5 eV (374.5 eV). The additional peak at lower binding energy can be attributed to the Ag−S component, in agreement with the corresponding S 2s chemical state of chemisorbed species (Figure 1d).[72,73] Not surprisingly, cysteine exposure for 3600 s leads to a general reduction of the Ag 3d intensity due to the attenuation of the Ag 3d photoelectrons through a thicker cysteine multilayer film on the surface. After annealing at 85 °C, there appears to be no discernible change in the Ag 3d peak widths, while the Ag $3d_{5/2}$ (Ag $3d_{3/2}$) peak at 368.5 eV (374.5 eV) shifts slightly to a lower binding energy of 368.4 eV (374.4 eV). The corresponding intensities for both Si−Ag and Ag−S features, however, increase due to partial desorption of the thick cysteine film. As desorption of the cysteine film continues upon further annealing to 175 °C and to 285 °C, the Si−Ag feature appears to reduce in intensity while the Ag $3d_{5/2}$ lower binding energy feature has further relocated to a slightly lower binding energy of 368.3 eV, which corresponds to the well-known metallic Ag−Ag (in the bulk).[74]

In a separate control experiment, we perform the same annealing procedure on a pristine Si(111)-$\sqrt{3}\times\sqrt{3}$-Ag surface (i.e., without any cysteine exposure). Evidently, the Ag 3d peak positions and areas of the single Ag−Si feature for Ag trimers of the pristine surface remain unchanged after each annealing step. There is no additional Ag−Ag feature emerged at a lower binding energy for this pristine Si(111)-$\sqrt{3}\times\sqrt{3}$-Ag sample.

These XPS results lead us to hypothesize the following model to account for the changes occurring to the cysteine multilayer film on the Si(111)-$\sqrt{3}\times\sqrt{3}$-Ag surface upon thermal evolution. In particular, chemisorption of cysteine on the Si(111)-$\sqrt{3}\times\sqrt{3}$-Ag surface creates Ag−S bonds involving a fraction of the Ag atoms on the surface. The formation of Ag−S bonds results in weakening of the Ag−Si bonds underneath and near the adsorption areas, potentially producing tension and strain. Annealing provides sufficient energy to overcome the activation barrier to further weaken and displace the Ag−Si bonds, creating interface defects. Meanwhile, reorganization of the cysteine molecules results in agglomeration of the displaced Ag atoms, leading to the formation of Ag clusters (or islands) with metallic Ag−Ag bonds. The formation of Ag clusters could account for the observed shift to a lower binding energy from the Ag 3d binding energy position of the Ag−S feature to that of the Ag−Ag feature upon annealing to 175 and 285 °C in Figure 2. Assuming no desorption and decomposition occurs at the interfacial layer (at 175 °C), the newly formed Ag clusters can be functionalized (either on top or around their perimeters) with the surrounding cysteine molecules of the interfacial layer. The disruption of the Si(111)-$\sqrt{3}\times\sqrt{3}$-Ag surface has also been observed for the adsorption of H atoms on the Si(111)-$\sqrt{3}\times\sqrt{3}$-Ag surface, in which the formation of Ag(111) agglomerates induced by the adsorption of H atoms at room temperature has also been reported.[75] It was claimed that the conversion process of $\sqrt{3}\times\sqrt{3}$-Ag to Ag metallic cluster could be reversed after (recombinative) desorption of H atoms at 500 °C. In our experiment, increasing the annealing temperature to 500 °C shows no change in the Ag 3d spectra in


DOI: 10.1021/acs.langmuir.9b02852
Langmuir 2019, 35, 16185−16200

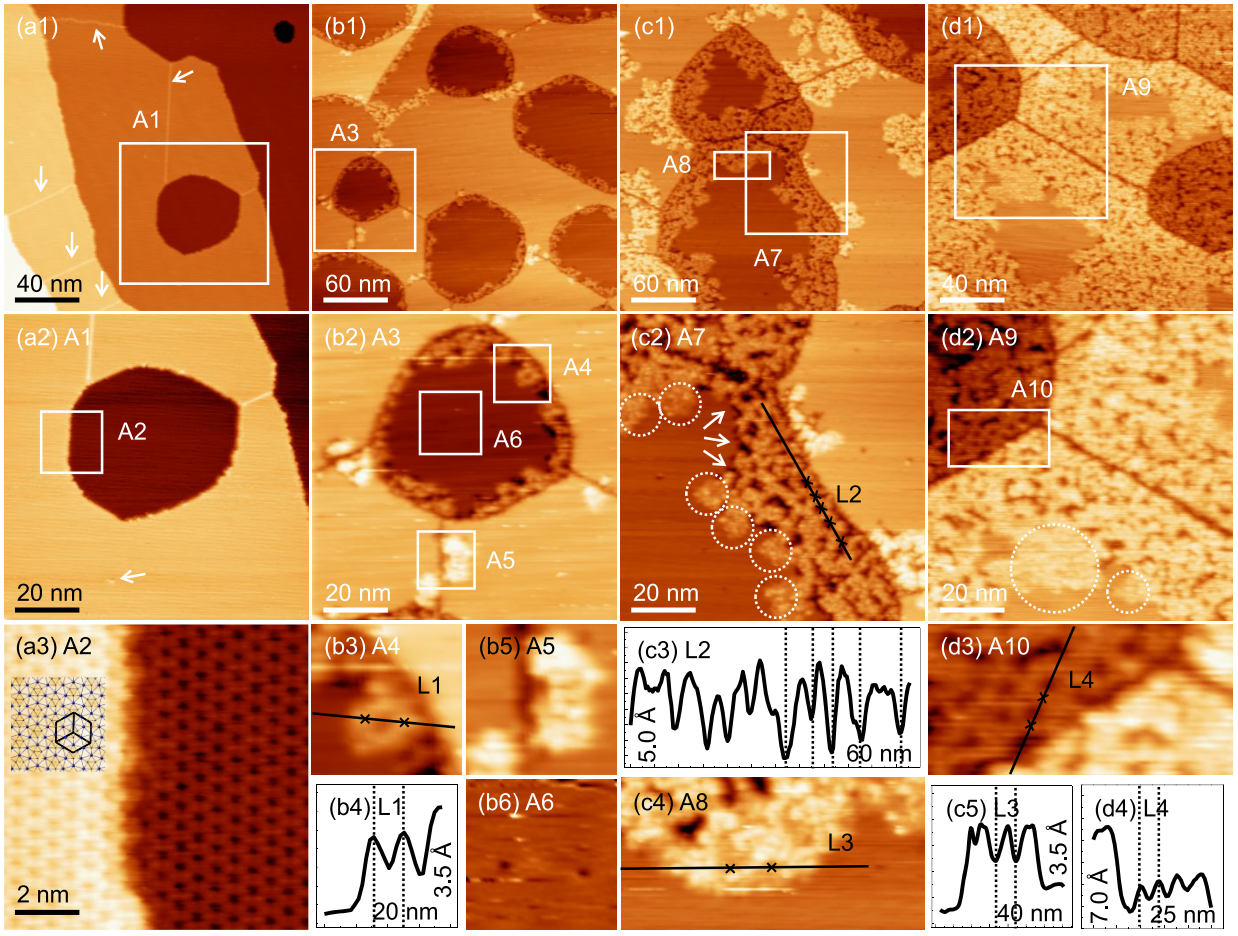


**Figure 3.** Empty-state STM images obtained with a sample bias of +2 V and a constant tunneling current of 0.2 nA for a pristine Si(111)-$\sqrt{3}\times\sqrt{3}$-Ag surface (a1−a3) before and after cysteine exposure for (b1−b6) 30, (c1−c5) 120, and (d1−d4) 240 s. Apparent height profiles along the respective lines are shown in b4, c3, c5, and d4, where the full height and length ranges are given in units of Angstroms and nanometers, respectively. Arrows in a1 and a2 mark examples of antiphase boundaries and adatom defects, respectively. Schematic model of the Ag−Si trimers hexagonal mesh along with three $\sqrt{3}\times\sqrt{3}$-Ag unit cells are overlaid on the image in a3, with the Ag and Si atoms represented by blue and gray dots, respectively.

Figure 2, which suggests that the H atoms resulted from dehydrogenation of cysteine are not the only cause of induced cluster formation. Evidently, the passivation of S or S-containing fragments enables the Ag clusters to remain stable to 500 °C. This is a significant result because thermal annealing of cysteine film on the $\sqrt{3}\times\sqrt{3}$-Ag overlayer provides a viable, nonreversible pathway of producing stable Ag nanoclusters. Further details of the surface morphology after annealing are discussed below.

**Preferential Early Stage Growth of Cysteine at Step Edges and Antiphase Boundaries on Si(111)-$\sqrt{3}\times\sqrt{3}$-Ag.** STM measurements have also been performed to investigate changes in the morphology of the Si(111)-$\sqrt{3}\times\sqrt{3}$-Ag surface upon low cysteine exposures, focusing on notable adsorption features particularly near step edges and antiphase boundaries in the early growth stage. Figure 3a1 shows the empty-state STM images of a pristine Si(111)-$\sqrt{3}\times\sqrt{3}$-Ag surface (i.e., before any cysteine exposure). The brighter and darker areas correspond to the upper step and lower step terraces, respectively, that are typically found on the Si(111)-$\sqrt{3}\times\sqrt{3}$-Ag surface.[76,77] In addition to these terraces, discernible step edges (between the upper step and the lower step terraces), antiphase boundaries (on the same terrace), and adatom and vacancy defects are also observed (Figure 3a1 and 3a2).[60] The high-resolution STM image of the surface shown in Figure 3a3 illustrates the expected honeycomb structure of the $\sqrt{3}\times\sqrt{3}$ surface reconstruction of Ag on Si(111). The Si(111)-$\sqrt{3}\times\sqrt{3}$-Ag surface structure has an oblique unit cell with side length $a = b = 0.7$ nm. Each unit cell contains three Ag atoms and three underlying Si atoms (appropriately arranged as illustrated in area A2, Figure 3a3). The step edge appears in the [1−21] and [110] directions, and the height of the step (or the rise) is 0.31 nm.[5,78] The step edges could appear either curved or straight with sharp angles depending on the surface preparation procedure.[79] The antiphase boundaries appear as straight bright lines in the STM image (Figure 3a1). The width of a typical antiphase boundary is 0.75 nm.[80]

After cysteine exposure for 30 s, the most significant changes can be found at the defect sites, which appear to be energetically the most favorable adsorption sites. As shown in Figure 3b1, the antiphase boundaries for the unoccupied surface states that usually appear brighter than their surrounding terrace sites have now become darker, indicating the changes in their electronic distribution upon cysteine adsorption. In addition, bright protrusions, attributed to cysteine adspecies, are found at step edges and antiphase boundaries. The adspecies are observed mostly at the lower



DOI: 10.1021/acs.langmuir.9b02852
Langmuir 2019, 35, 16185−16200

step edges rather than the upper step ones, indicating the higher reactivity of the lower step edges and the absence of Ehrlich−Schwoebel barrier at the upper step edges. All of the areas in the immediate proximity of the lower step edges are consistently populated with adspecies with a nearly uniform width, suggesting continuous diffusion and adsorption and consequently leading to nearly the same growth rates in all directions. In the magnified area A3 (Figure 3b2), the majority of the adsorbates at the lower step edge appear as clusters, while area A6 on the lower step terrace (and other upper step terrace, Figure 3b2) appears to contain isolated bright protrusions and isolated dark depressions (Figure 3b6). The majority of the clusters in area A4 appear to aggregate into a ring with a depression at the center (Figure 3b3). According to the height profile along line L1 (Figure 3b4), the size of its constituent moieties is consistent with the size of those measured on the isolated single bright protrusions in area A6 and elsewhere (Figure 3b2 and 3b6). These isolated single bright protrusions may therefore be considered as the building blocks of the ring-like clusters, and the apparent depression in the center (Figure 3b3) could indicate the gap between the adsorbates. Similar to the lower step edges, antiphase boundaries also appear to be more favorable to adsorption than the upper step edges and bare terraces. Similar behavior of cluster formation is observed at the edges of the antiphase boundaries in area A5 (Figure 3b2 and 3b5). The chain-like structure of the antiphase boundaries appears to be affected by the adsorbates as manifested through reduction of their apparent height. A closer look at the terrace sites in area A6 (Figure 3b2 and 3b6) reveals the presence of individual dark depressions that are similar in size to those of individual bright protrusions. These dark depressions can also be found near the perimeters of the adsorbate islands at the step edges and antiphase boundaries. As in an earlier report on the chemisorption of ferrocene on Si(111)-$\sqrt{3}\times\sqrt{3}$-Ag, both the presence of individual dark depressions on the terrace sites and a lower apparent height at the antiphase boundaries could be attributed to chemisorption of the adspecies.[23]

Not surprisingly, the bright protrusions corresponding to the cysteine adspecies increase in population and become more extended in size with increasing cysteine exposure from 30 (Figure 3b1) to 120 (Figure 3c1) and 240 s exposures (Figure 3d1). Evidently, the adsorbate islands become larger both in area and in apparent height, and they appear grainier and more porous in texture with increasing exposure time. The most prominent feature of the adsorbate islands appearing at these intermediate coverages is the spreading of the networks of protrusions interconnecting to one another forming a porous structure that resembles the coral reef. The grainy protrusion appearance of the adsorbate islands leads to pores that could potentially include both the gaps in the ring-like clusters and the chemisorption-induced dark depression areas (Figure 3c2 and 3d2). In area A7 (Figure 3c1 and 3c2), the entire region along the lower step edge is covered with adspecies, while only a few small islands are found at the upper step edge. The height profile along line L2 over a chain of dark depressions on the adsorbate island near the lower step edge (Figure 3c3) illustrates the typical roughness of the adsorbate island. Interestingly, there appears to be some approximate regularity in the spacing between the pores, which suggests possible short-range ordering in the adsorption induced by the step edge. The widths of the islands near the step edges increase by nearly the same extent on both the lower step terraces and the upper step terraces after the 240 s exposure (Figure 3d1). As the lower step terraces occupy smaller footprints of the overall surface (depending on the sample preparation), these terraces are completely occupied by the adspecies first before the upper step terraces (Figure 3d1).

As the island growth extends deeper into a terrace region and away from the nearby step edge or antiphase boundary region, a lower density of dark depressions and an apparently much smoother appearance for the areas (marked with dotted circles in both area A7 in Figure 3c2 and area A9 in Figure 3d2) are found, confirming that a higher number of adsorbate-induced pores are formed largely on the terrace regions near the step edges. This in turn suggests that the nature and morphology of the step-edge sites play an important role in imprinting structural relations in the adsorption pattern of these adspecies near the step edges. Indeed, the pore sizes of the ring-like clusters in area A4 (Figure 3b3) and in area A10 (Figure 3d2 and 3d3) are found to be quite similar, as shown in their respective height profiles along lines L1 (Figure 3b4) and L4 (Figure 3d4). This suggests similar nature of these ring-like clusters, with their formation likely induced by adsorption near the step edges and their growth in population with increasing exposure. This in turn supports the notion of the presence of a structural relation near the step edges. On the other hand, this structural relation becomes weaker and is lost for adspecies located farther and farther away from the step edges. For the smoother island far away from the step edges in area A8 (Figure 3c1 and 3c4), the height profile along line L3 (Figure 3c5) shows mainly two different apparent heights of adsorbates, suggesting the presence of a second adlayer in this area similar to the areas near the step edges.

Nucleation and growth of cysteine islands do not appear to initiate on the generally defect-free terraces, which could be caused by the large diffusivity of the cysteine molecules at room temperature (due in part to the high activation barrier for dehydrogenation of the thiol group) and to the relatively small size of the terraces when compared to the large transport length of surface diffusion on the Si(111)-$\sqrt{3}\times\sqrt{3}$-Ag surface.[23,81] The initial adsorption at non-terrace sites indicates that defect sites are energetically more favorable to activate dehydrogenation of the thiol group. In Figure 4 we show a schematic model of the adsorption mechanism for cysteine on the Si(111)-$\sqrt{3}\times\sqrt{3}$-Ag surface, which we consider to involve four main structural components: lower step terrace, upper step terrace, step edge, and antiphase boundary (as illustrated in Figure 4a). For the step edge, we could consider adsorption on the lower step edge, upper step edge, and slope surface [where the slope corresponds to the rise (vertical displacement) over the run (horizontal displacement)]. Upon arriving on the terraces (both lower step and upper step terraces), the cysteine molecules are free to diffuse on the terrace sites until they arrive at the step edges or antiphase boundaries (Figure 4a). We obtain more direct evidence of this surface diffusion in a series of time-sequence STM images in Figure S3, which shows the addition of bright protrusions to the edges of the adspecies islands at room temperature over the collection time of a set of STM images collected one after another. Cysteine molecules undergo dissociative adsorption with S−H bond cleavage and S−Ag bond formation, and the resulting dehydrogenated adspecies (thiolated cysteine) become trapped at these defect sites (Figure 4b). Anchoring to the surface through their thiolate groups, the dehydrogenated cysteine adspecies with their free amino and carboxylic acid groups



DOI: 10.1021/acs.langmuir.9b02852
Langmuir 2019, 35, 16185−16200

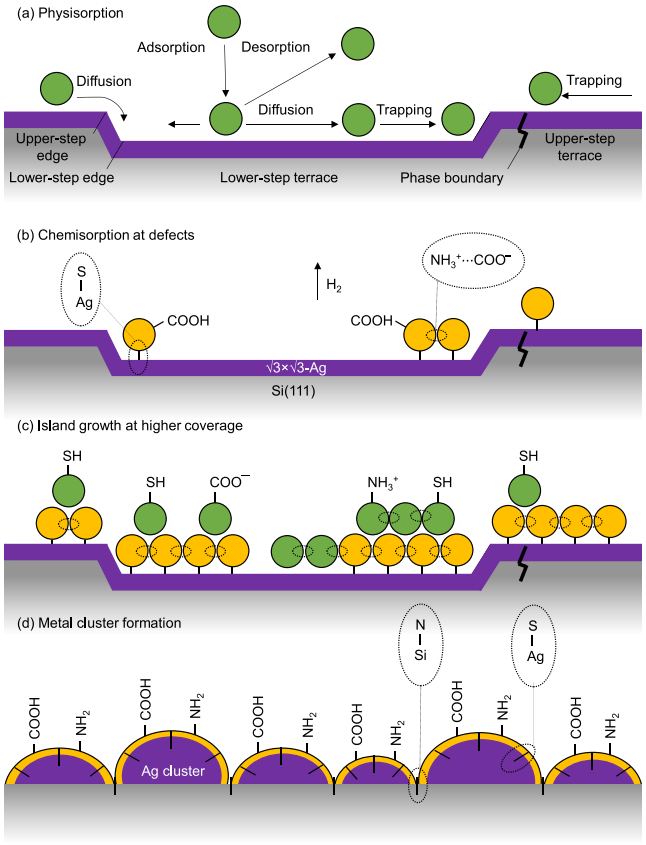


**Figure 4.** Schematic illustration of (a–c) adsorption and growth of cysteine adspecies on the Si(111)-$\sqrt{3}\times\sqrt{3}$-Ag surface at room temperature and (d) metal cluster formation after annealing. Green and yellow balls depict undissociated cysteine molecules and thiolated cysteine molecules, respectively. Purple layers in (a–c) represent the $\sqrt{3}\times\sqrt{3}$-Ag overlayer, which converts to metallic clusters in (d).

provide new linkage points for further attachment of other molecules through zwitterionic interactions and thus propagate growth of the adspecies islands both laterally and vertically (Figure 4c). Our XPS results show that loosely bound species start to appear at the submonolayer coverage, which we attribute to the onset of second-layer adsorption while the interfacial layer chemisorption is still developing. The emergence of second-layer adspecies is corroborated by our STM measurement. Among all of the defect sites, the lower step edges provide the most reactive sites for adsorption, followed by the antiphase boundary sites and then the upper step edges. Figure 4d shows a schematic model of the as-grown cysteine thick film surface after annealing. STM images of the surface morphology obtained after annealing will be shown in the following section.

The high mobility of the molecular building blocks is a prerequisite for the formation of self-assembled nanostructures on the terraces of solid surfaces. On the other hand, the reactivity of the molecule (arising from different functional groups) and its size relative to the separations of various available adsorption sites play an important role in the competition between molecule–molecule and molecule–substrate directional interactions for constructing the supramolecular architectures.[82] On the semimetallic Si(111)-$\sqrt{3}\times\sqrt{3}$-Ag surface, no ordered nanostructure is seen in the interfacial layer (from our STM images). However, the imprinting of the Si(111)-$\sqrt{3}\times\sqrt{3}$-Ag surface template is observed in areas near the step edges as irregular ring-like clusters that contribute to the porous (coral reef like) morphology at higher coverages. To understand the adsorption of the cysteine molecules in more detail, we perform DFT calculations to determine its adsorption configurations on the terrace sites of the Si(111)-$\sqrt{3}\times\sqrt{3}$-Ag surface (discussed below). More detailed calculations about the adsorption on the defect sites on step edges and antiphase boundaries of the surface will be given elsewhere.

**Formation of Silver Nanocluster Arrays by Post-annealing.** Our XPS results show that annealing the Si(111)-$\sqrt{3}\times\sqrt{3}$-Ag surface pre-exposed with cysteine at elevated temperatures leads to emergence of the Ag metallic state,

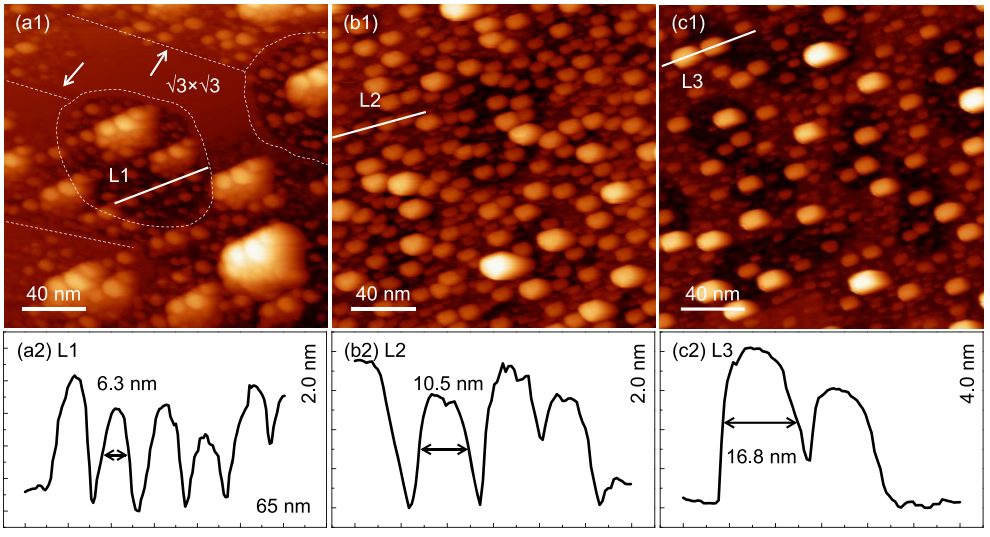


**Figure 5.** Empty-state STM images obtained with a sample bias of +2 V and a constant tunneling current of 0.2 nA for Ag nanocluster arrays obtained by postannealing a Si(111)-$\sqrt{3}\times\sqrt{3}$-Ag surface with cysteine exposures of (a1) 240 and (b1, c1) 3600 s at (a1) 175, (b1) 285, and (c1) 500 °C, respectively. Apparent height profiles along the respective lines L1, L2, and L3 are shown in a2, b2, and c2, respectively. *x*-axis scale ranges for all height profiles are 65 nm. *y*-axis scale ranges for the L1, L2, and L3 height profiles are 2.0, 2.0, and 4.0 nm, respectively.



DOI: 10.1021/acs.langmuir.9b02852
*Langmuir* 2019, 35, 16185–16200

indicating significant changes in the electronic structure of the $\sqrt{3}\times\sqrt{3}$-Ag surface template. To confirm our Ag 3d XPS results (Figure 2), we collect the STM images after annealing the as-grown cysteine films with submonolayer and multilayer coverages supported on the $\sqrt{3}\times\sqrt{3}$-Ag surface. Figure 5a1 shows the morphology of the surface with a 240 s cysteine exposure (a submonolayer coverage) upon annealing at 175 °C. The porous coral-reef-like nanostructures of the cysteine adsorbate islands initially observed before annealing (Figure 3d1) are no longer present after annealing. Instead, the surface is partly covered with larger bright protrusions with an apparent diameter of 3.2−10.5 nm, as illustrated in the height profile along line L1 in Figure 5a2. Since the adspecies coverage is less than one monolayer initially, some parts of the pristine $\sqrt{3}\times\sqrt{3}$ surface are not covered by adspecies and are therefore exposed. These areas remain intact after annealing as evidenced by the appearance of smooth terraces (marked by $\sqrt{3}\times\sqrt{3}$) and typical antiphase boundaries (marked by arrows) in Figure 5a1. Selected magnified areas of Figure 5a1 showing the smooth $\sqrt{3}\times\sqrt{3}$ surface terrace, the step edge, and the antiphase boundary are illustrated in Figure S4. This therefore indicates that only the areas covered by the cysteine adsorbate islands are affected by annealing at an elevated temperature. The clusters (bright protrusions) appear to have agglomerated to form larger clusters or islands. The appearance of these new STM features, i.e., clusters and islands, are corroborated with the emergence of the metallic Ag $3d_{5/2}$ peak at 368.3 eV after annealing at 175 °C (Figure 2), which can therefore be used to validate the metallic nature of these clusters. Annealing the Si(111)-$\sqrt{3}\times\sqrt{3}$-Ag surface covered with a multilayer of cysteine (with a 3600 s exposure) at a higher temperature of 285 °C results in a much denser layer of bright protrusions without any part of the smooth $\sqrt{3}\times\sqrt{3}$-Ag surface visible, which is consistent with the surface fully covered by cysteine before the annealing (Figure 5b1). Evidently, these bright protrusions exhibit a narrow size distribution, with the larger clusters formed by agglomeration of the smaller clusters. The majority of the clusters appear to exhibit an apparent size of 6.3−15.3 nm, as illustrated by the height profile along line L2 in Figure 5b2. In order to compare our STM results with those reported for cluster formation induced by hydrogen adsorption,[83−85] we increase the annealing temperature to 500 °C, and the result is shown in Figure 5c1. Evidently, the metal clusters persist and do not disappear after annealing at 500 °C. It should be noted that 500 °C corresponds to the nominal annealing temperature required to produce the $\sqrt{3}\times\sqrt{3}$ Ag overlayer from an as-deposited monolayer of Ag on Si(111). In marked contrast to adsorbed H-induced clusters reported earlier,[83−85] the smooth $\sqrt{3}\times\sqrt{3}$ structure cannot be restored by annealing and the present cluster formation is therefore robust and not reversible. This indicates the encapsulation of the Ag metallic clusters and the local passivation of the underlying Si layer by S (from the dehydrogenated thiol group) and N (from the dehydrogenated amino group) consistent with our XPS results. This further suggests that the supported metal clusters resulted from cysteine adsorption and the subsequent annealing process are stable even at higher temperature.

The clusters also appear to organize with short-range alignment in a preferred direction as shown in Figure 5a1−5c1. This limited directionality is likely guided by both the imprinting effect of the underlying Si surface and the presence of cysteine adspecies (molecules or decomposition fragments) in between or at the perimeters of the clusters. The alignment of Ag clusters along the crystallographic directions of the Si(111) surface has also been reported for adsorption of Ag on H-terminated Si(111) surface.[86] As the metal clusters are functionalized (at their perimeters) by cysteine adspecies, the interactions among these adspecies could enable semi-ordering among the clusters along certain preferred directions. The use of cysteine to generate aligned nanocluster arrays on Si(111) promises a new approach to synthesize nanocatalysts and/or nanocluster templates.

**Large-Scale DFT Calculations of Cysteine Adsorption on Model Si(111)-$\sqrt{3}\times\sqrt{3}$-Ag Surface.** Cysteine exists as a free molecule in numerous stable structures in the gas phase. Of the 324 possible conformers calculated for both L- and D-cysteine, 42 are considered the most stable due to the presence of different types of internal hydrogen bonding among their functional groups.[87] Through interaction with different surface atoms of the substrate (at different surface sites), some of these cysteine conformers may become more favorable for direct adsorption while others may undergo rearrangement upon adsorption on the $\sqrt{3}\times\sqrt{3}$-Ag surface. A variety of adsorption structures/configurations at the substrate sites could provide local energy minima and are therefore energetically plausible. Given the inherent complexity of the system at hand and the lack of information about preferred orientations of the functional groups with respect to a specific surface site, we begin our calculations by first selecting three energetically most stable L-cysteine conformers. Figure 6a shows the equilibrium

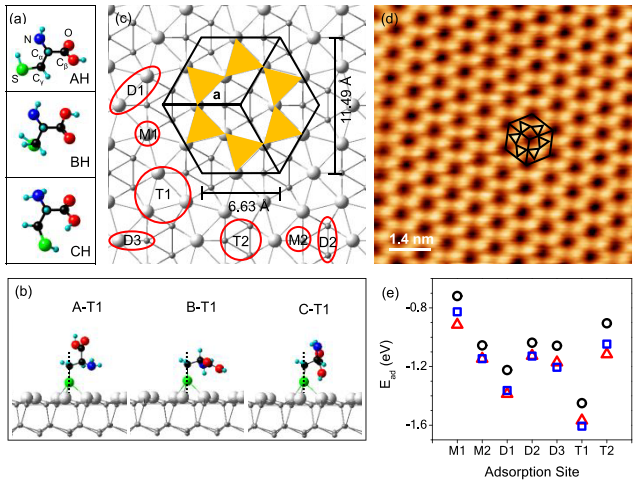


**Figure 6.** (a) Optimized equilibrium structures of three conformers (AH, BH, and CH) of isolated L-cysteine in the gas phase. (b) Side view of the adsorption configurations of three dehydrogenated cysteine conformers A, B, and C on the T1 site with the S−C axis along the surface normal. (c) Top view of the Si(111)-$\sqrt{3}\times\sqrt{3}$-Ag surface illustrating prospective adsorption sites, including the 3-fold hollow sites on Ag trimer (T1) and Si trimer (T2), bridge sites on Ag−Ag (D1), Si−Si (D2), and Ag−Si nearest neighbor pairs or dimers (D3), and atop sites on top of a Ag atom (M1) and a Si atom (M2). (d) Three $\sqrt{3}\times\sqrt{3}$-Ag unit cells overlaid on top of an empty-state STM image of a pristine Si(111)-$\sqrt{3}\times\sqrt{3}$-Ag surface obtained with a sample bias of +2 V and a constant tunneling current of 0.2 nA. (e) Calculated adsorption energies of dehydrogenated cysteine conformers A (circles), B (squares), and C (triangles) on adsorption sites M1, M2, D1, D2, D3, T1, and T2 optimized by varying the molecule-to-slab vertical separation while holding all other structural parameters fixed.



DOI: 10.1021/acs.langmuir.9b02852
Langmuir 2019, 35, 16185−16200

structures for three isolated L-cysteine conformers, with conformer AH being 0.06 and 0.13 eV more stable than conformers BH and CH, respectively. In accord with our XPS results that show the adsorption being dominated by bonding to the surface through the dissociated thiol group, we therefore only consider anchoring the S end to the surface in our adsorption configuration calculations. After removing the H from the thiol group, we orient the three gas-phase thiolated conformers with their respective S−C axis perpendicular to the $\sqrt{3}\times\sqrt{3}$-Ag surface to obtain three initial adsorption structures with the carboxylic acid group pointing upward (conformer A), parallel (conformer B), and downward (conformer C) with respect to the surface plane, as shown in Figure 6b. To qualitatively identify the more stable surface adsorption sites, we place a single thiolated cysteine conformer at a selected adsorption site through its thiolate group. A near-optimized adsorption configuration is then obtained by relaxing just the separation between the adspecies and the site in the $z$ direction while keeping the adspecies and the slab frozen at their separately optimized equilibrium structures.

Figure 6c shows the probable adsorption sites that include the atop sites on top of a Ag monoatom (M1) and a Si monoatom (M2), the bridge sites on a Ag−Ag dimer (D1), a Si−Si dimer (D2) and a Ag−Si dimer (D3), and the 3-fold hollow sites on a Ag trimer (T1) and a Si trimer (T2). The hexagon pictogram containing three $\sqrt{3}\times\sqrt{3}$ surface unit cells, each with two constituent Ag trimers, is highlighted on the surface model in Figure 6c and on our atomically resolved STM image in Figure 6d. It should be noted that a bright protrusion in the honeycomb network observed in the STM image (Figure 6d) corresponds to a Ag trimer as marked by a solid triangle in Figure 6c. The calculated adsorption energies for the three thiolated cysteine conformers on these adsorption sites are compared in Figure 6e. The adsorption energy ($E_{ad}$) of a thiolated cysteine conformer on a selected site of the slab is given by

$$E_{ad} = E_{M-slab} - E_{slab} - E_{M}$$

where $E_{M-slab}$, $E_{slab}$, and $E_{M}$ are, respectively, the equilibrium energies of the adsorbate−substrate system, the slab (used as the model substrate), and the thiolated cysteine radical ($\bullet SCH_2CHNH_2COOH$) in the gas phase. This definition of the adsorption energy corresponds to the bond formation between the thiolated cysteine radical and the surface, i.e.

$$(\bullet SCH_2CHNH_2COOH) + \text{Surface} \rightarrow \text{Surface}-SCH_2CHNH_2COOH$$

In the present definition, we have avoided the need to consider the dissociation energies of cysteine and hydrogen molecules. As the main goal of the present computational study is to identify notable trends in the adsorption configurations of plausible thiolated cysteine conformers, this definition of the adsorption energy is more practical. Evidently, the most favorable adsorption site (with the most negative adsorption energy) for all three conformers is found to be the T1 site, followed by the D1 site, with a 0.2 eV less negative adsorption energy. The energy differences among the three conformers for a particular site are generally small. While the adsorption energies of conformers B and C on the T1, D1, D2, D3, and M2 sites are nearly the same (within 0.06 eV), those of conformer A are discernibly higher (by 0.2 eV). Conformer A is also the least stable one for all of the adsorption sites, which confirms that orienting the carboxylic acid group upright and away from the surface (without benefiting from auxiliary interactions of the carboxylic acid and amino groups as in conformers B and C) would lead to less stable adsorption configurations. Cysteine also prefers adsorption on a bridge or 3-fold hollow Ag sites rather than the corresponding Si sites, which is supported by the observed shift in the S 2s binding energy to a lower energy. This is, however, in marked contrast to the bond energy of S−Si (292.9 kJ/mol)[88] being higher than that of S−Ag (216.7 kJ/mol).[89] This apparent bond energy advantage is not relevant here because of the relative position of the Ag trimers being 0.8 Å above the Si trimers (on the terraces) and of the steric hindrance of the cysteine molecules, making the Si sites less accessible for adsorption. In addition, the dangling bonds of Si atoms are already saturated through bonding with other Si atoms and Ag atoms and therefore not available to interact with any adspecies.

In order to determine the effect of the other two functional groups on the stabilization of the adsorption energy, we reoptimize the adsorption geometries with the structures of both the slab and the adsorbate fully relaxed. Tables S2−S4 show the adsorption configurations and adsorption energies before and after relaxation for conformers A, B, and C at the trimer, dimer, and monomer sites, respectively. Interestingly, all three conformers have relocated to the D1 sites when initially placed on the M1, M2, D1, and D3 sites. Initial placement on D2 and T2 has changed to M1 for all three conformers, except for conformer C initially on T2, which has changed to D1. Initial placement on T1 sites remains the same for conformers B and C, while conformer A has moved to D1 after full geometry optimization. Clearly, none of the Si related sites (M2, D2, T2) has led to stable adsorption upon complete optimization for all three conformers. For the Ag-related sites (M1, D1, D3, T1), the D1 site has become the most favorable adsorption site after relaxation for all three conformers (with small variations in the structural parameters), with 67% of all of the adsorption configurations relaxed into the D1 configurations. We summarized the most stable, fully optimized adsorption geometries of all three conformers on the D1 sites in Figure 7 (top panel). While the adsorption energies for the A−D1 and B−D1 configurations are within 10% of each other, that for the C−D1 configuration is discernibly less negative (i.e., less stable). For conformers B and C initially placed on the T1 sites, complete optimization has not affected the adsorption sites (T1) but has improved the adsorption energies. However, conformer A initially placed on the T1 site has apparently moved to the nearest D1 site (Figure 7, bottom panel). Not surprisingly, the fully optimized configurations for all three conformers on the M1 site, with the adsorption energy of A−M1 being the least negative, are generally less stable than those on the T1 and D1 sites. On Ag(111), the stability of the thiolated cysteine adsorption has been found to increase from the atop, to bridge, and to 3-fold hollow sites.[41] A detailed DFT study of L-cysteine adsorption at the bridge sites of the Ag(111) surface has revealed a complicated interplay between sp and d states of silver in the bond formation between the adsorbate and the surface. Bridge sites have also been reported to be the most favorable adsorption sites for thiolated cysteine on Au(111)[53,54] and Au(110),[47,57] where flat adsorption configurations with S−Au at an off-bridge site and $NH_2$−Au at an off-atop site were found to be energetically more favorable on the Au(111) surface.



DOI: 10.1021/acs.langmuir.9b02852
Langmuir 2019, 35, 16185−16200

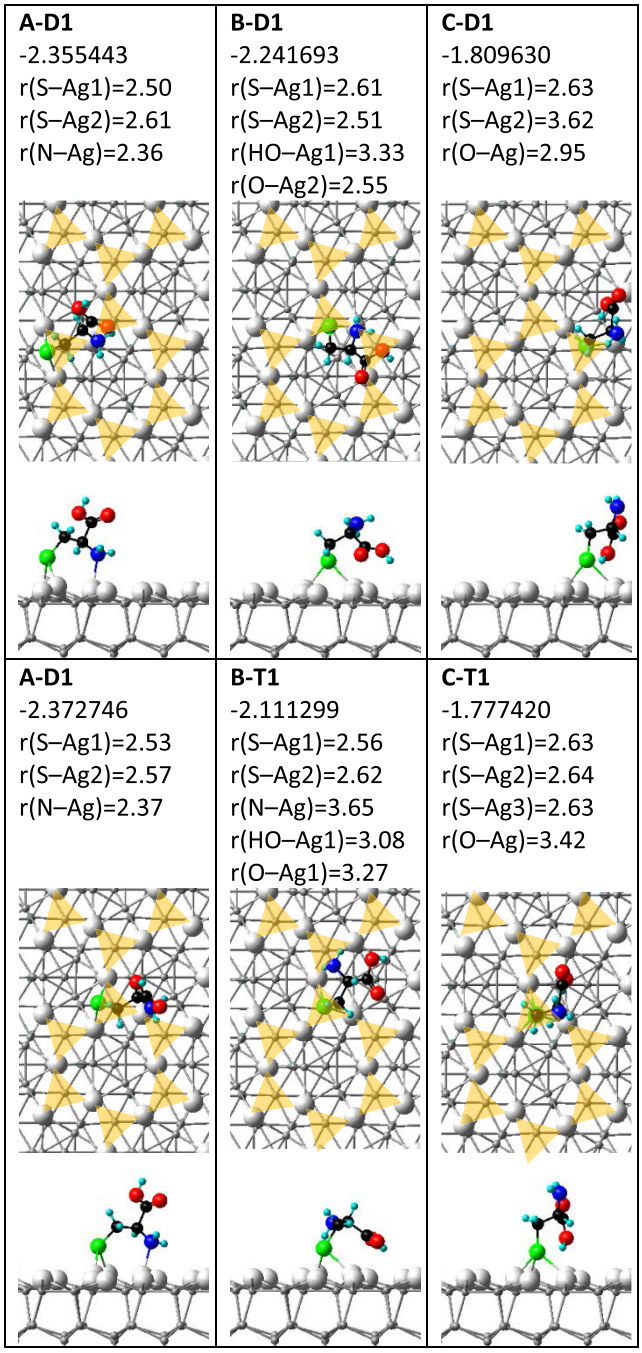


**Figure 7.** Top views and side views of the equilibrium geometries of optimized adsorption configurations after full relaxation of thiolated cysteine conformers A, B, and C initially placed on D1 (top panels) and T1 sites (bottom panels) of the Si(111)-$\sqrt{3}\times\sqrt{3}$-Ag model surface. Adsorption structures (and the notations) correspond to the final optimized results after relaxation. Adsorption energies are in unit of electron volts, while the separations $r$(X–Y) are in unit of Angstroms. To better illustrate the adsorption structure, only part of the slab (that corresponds to the full 4×4 supercell) for the model surface is shown for each configuration.

According to the adsorption energies for all three conformers after full relaxation, conformer A has become the most favorable conformer of thiolated cysteine for adsorption on these sites, which suggests that complete geometry optimization (relaxation) allows thiolated cysteine to be repositioned to enable the amino group to play a stabilizing role. The magnitudes of the adsorption energies of the conformers appear to follow a trend [A (most negative and most stable) < B < C (least negative and least stable)] that is opposite to that of the separations between the amino groups in these conformers and the surface. Upon relaxation of the atomic positions, the S–C axis that is set initially perpendicular to the surface plane is now tilted, enabling the amino group to lean toward the Ag atoms of the surface. The tilt in the S–C axis is also found for conformer B, while it remains unchanged for almost all adsorption configurations of conformer C, which could account for the lower stability of conformer C as compared to other two conformers.

**Large-scSale DFT Calculations of Cysteine Zwitterionic Multimers on Model Si(111)-$\sqrt{3}\times\sqrt{3}$-Ag Surface.** To investigate the effect of intralayer bonding involving other functional groups that are not used for direct attachment to the surface on the adsorption, we perform calculation of other plausible adsorption geometries in which either the amino or the carboxylic acid or both groups are initially close to the surface. This type of calculations could provide some insights into the early formation of the zwitterionic layer of cysteine on the Si(111)-$\sqrt{3}\times\sqrt{3}$-Ag surface. While the A–D1 configuration with the carboxylic acid group pointing away from the surface is more conducive to initiating bonding with the second adlayer, a small rotation of the $C_\alpha$–C bond could reposition the carboxylic acid group such that it becomes more accessible to intralayer bonding in the first adlayer. Figure 8a and 8b shows the optimized geometries of the most favorable A–D1 adsorption configurations, where the C–$C_\alpha$–C plane is tilted parallel to the surface, with $H_\alpha$ (the H atom connected to $C_\alpha$) pointing up away from and down toward the surface, respectively. The separations between the functional groups and the respective underlying silver atoms are $r$(S–Ag1) = 2.54 Å, $r$(S–Ag2) = 2.64 Å, $r$(N–Ag) = 2.42 Å, and $r$(O–Ag) = 3.52 Å for the $H_\alpha$-up configuration and $r$(S–Ag1) = 2.57 Å, $r$(S–Ag2) = 2.57 Å, $r$(N–Ag) = 2.41 Å, and $r$(HO–Ag) = 3.32 Å for the $H_\alpha$-down configuration. Both A–D1 configurations in Figure 8a and 8b as well as the upright A–D1 configuration in Table S3 are consistent with our XPS data, which support the presence of free amino and carboxylic acid groups at low coverages. As expected, the configuration with the molecular plane more surface parallel (Figure 8a) is energetically more stable (by 0.1 eV) due to the potential interaction of lone-pair electrons of the amino group with the surface Ag atoms. Such a more surface-parallel A–D1 configuration is a strong candidate for cysteine adsorption at very low coverage, in good accord with experimental and theoretical reports of cysteine on Au(110)[47] and Ag(111) surfaces[41] at low coverages.

Using the A–D1 surface-parallel adsorption configuration (Figure 8a), we calculate the adsorption configuration for cysteine dimer obtained with addition of a thiolated cysteine conformer (A) in appropriate orientation (Figure 8c). On the Au(111) and Au(110) surfaces, cysteine dimer formation has been reported to be as favorable as the single molecule adsorption at low coverages.[47,53,54,58] The cysteine dimer in Figure 8c is therefore another prospective candidate for adsorption at lower coverages, in good accord with our XPS results in which both zwitterionic and neutral states are observed. Under UHV condition, zwitterions have been observed at higher coverages, where their formation is driven by the intermolecular proton transfer between the hydroxyl group of one molecule and the amino group of a neighboring molecule.[39,40,52,53] A common DFT approach used to



DOI: 10.1021/acs.langmuir.9b02852
Langmuir 2019, 35, 16185–16200

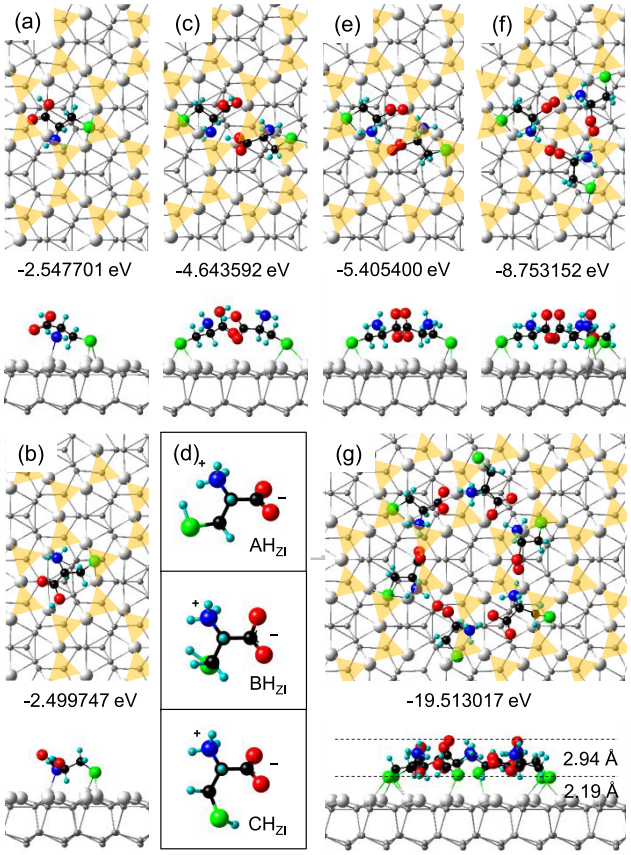


**Figure 8.** Equilibrium geometries and adsorption energies of optimized adsorption configurations on D1 sites for thiolated conformer A with (a) $H_\alpha$ up and (b) $H_\alpha$ down, (c) hydrogen-bonded dimer containing two thiolated neutral conformer A with $H_\alpha$ up, (e) dimer containing two thiolated zwitterions $A_{ZI}$, (f) trimer containing three thiolated zwitterions $A_{ZI}$ with $H_\alpha$ up, and (g) hexamer containing six thiolated conformers $A_{ZI}$ with $H_\alpha$ up. (d) Equilibrium geometries of isolated zwitterions (ZIs) for conformers AH, BH, and CH. Thiolated zwitterion $A_{ZI}$ is derived by proton relocation from COOH to $NH_2$ in a thiolated conformer A. To better illustrate the adsorption structure, only part of the slab (which corresponds to the full 4×4 supercell for a−c and e and f and to the full 8×8 supercell for g) for the model surface is shown.

determine the coverage-dependent zwitterionic structure formation is to first calculate the adsorption configuration of a single molecule on the surface in a sufficiently large supercell corresponding to the low coverage regime. Decreasing the cell size appropriately would then promote highly ordered zwitterionic intermolecular interactions and therefore can be used to mimic the higher coverage regime. In our system, however, the zwitterionic chemical state is observed even at very low coverages due to the presence of high densities of step edges and small terraces as well as to the high diffusivity of cysteine on Si(111)-$\sqrt{3}\times\sqrt{3}$-Ag. As we do not observe any ordered structure of cysteine at any coverage, the aforementioned approach of calculating the zwitterionic intermolecular interaction is less effective. We therefore used a thiolated form of the zwitterion of conformer $AH_{ZI}$ (shown in Figure 8d) as the initial form of the adsorbate to redo the calculation for the adsorption configuration of the cysteine dimer (involving zwitterionic interactions between deprotonated carboxylic acid and protonated amino groups of one cysteine zwitterion with the respective protonated amino and deprotonated carboxylic acid groups of a neighboring cysteine zwitterion). We obtain the equilibrium geometry of an adsorption configuration (Figure 8e) that is similar to that shown in Figure 8c with slight differences in the orientation of the $-NH_3^+\cdots COO^-$ components and their separations. The corresponding adsorption energy is found to be more negative by 0.75 eV relative to the non-zwitterionic dimer, which confirms that the zwitterionic dimer form is more stable than the neutral dimer form. This is reasonable because the cysteine dimer in Figure 8e is stabilized by two mutual zwitterionic hydrogen bonding, while the one in Figure 8c contains only one hydrogen bond. Using the latter approach, we also calculate other possible zwitterionic dimers, including dimer of conformer AH with $H_\alpha$ down and dimer of conformer BH (Figure S5), which are found to have less negative adsorption energies than that shown in Figure 8e. Figure 8f and 8g shows the calculated adsorption configurations of the zwitterionic trimer and zwitterionic hexamer, respectively. These zwitterionic structures of cysteine dimer, trimer, and hexamer found in our calculations are consistent with some of the notable protrusion features observed in our STM data, Figure 3b3 and 3d3. The respective $-NH_3^+\cdots COO^-$− bond lengths of these zwitterionic bonds are found to be 1.67 (dimer), 1.55 (trimer), and 1.73 Å (hexamer), which are in general accord with previous DFT calculations of cysteine on other surfaces.[39,58] Using the vertical separation between the topmost O atom of the cysteine adsorbates and the Ag atom underneath, the thickness of the interfacial layer with flat configuration is calculated to be 5.13 Å (Figure 8g). This estimate of the interfacial layer thickness is used for calculating the coverage of chemisorbed species in the interfacial layer based on our XPS data discussed above. It should be noted that minor displacements in the Ag positions in the $\sqrt{3}\times\sqrt{3}$-Ag template are also observed for dimer, trimer, and hexamer adsorption configurations.

The calculated hexamer structure (and larger multimer structures, not shown) for the D1 site on the terrace is therefore inspired by the ring-like structures at low coverage found in our STM images in Figure 3b3 and 3d3. While individual cysteine adspecies involved in forming each ring are too small to be resolved in our STM images, the calculated adsorption configurations shown in Figure 8 illustrate the viability of zwitterionic multimer structures for use as the building blocks in the cysteine film growth on the Si(111)-$\sqrt{3}\times\sqrt{3}$-Ag surface. This type of large-scale DFT calculations is therefore especially important for verifying the presence of zwitterionic intermolecular interactions, in addition to the molecule-to-substrate covalent bonding at the interfacial layer for corroborating with both our XPS and STM results.

## CONCLUSION

The $\sqrt{3}\times\sqrt{3}$-Ag reconstruction on the Si(111)7×7 surface offers a unique, single-atom-thick, two-dimensional metal silicide platform to investigate the surface chemistry of biomolecules. With a variety of bonding sites available not just on its lower step terraces and upper step terraces but also on step edges and antiphase boundaries, the Si(111)-$\sqrt{3}\times\sqrt{3}$-Ag surface provides a rich test bed for studying site-specific chemistry, particularly the role of defects. As one of two natural S-containing amino acids, cysteine offers three important functional groups to explore the surface chemistry of these bonding sites. In the present work, we follow the growth of a cysteine nanofilm and study their interfacial interactions with the Si(111)-$\sqrt{3}\times\sqrt{3}$-Ag surface and their molecule-to-



DOI: 10.1021/acs.langmuir.9b02852
*Langmuir* 2019, 35, 16185−16200

molecule interactions. By combining the results from our XPS and STM experiments with complementary large-scale DFT calculations, we are able to decipher the chemical nature of the interface and reach a molecular level understanding of the physical processes occurring in such an intricate system. Adsorption of cysteine is found to begin on the lower step edge and antiphase boundary sites and the adsorption fronts propagate from these defect sites out to the terrace regions with increasing exposure. This result suggests the viability of preferential site functionalization by manipulating the formation of and adsorption on specific defect sites of the Si(111)-$\sqrt{3}\times\sqrt{3}$-Ag surface. We propose a plausible diffusion-driven adsorption model for the observed growth evolution. Unlike the cysteine film growth on Si(111)7×7, no transitional layer is observed on Si(111)-$\sqrt{3}\times\sqrt{3}$-Ag at room temperature, as supported by the absence of hydrogen bonding found in our XPS spectra obtained at low exposures. The zwitterionic structures therefore start on the interfacial layer and grow directly onto the multilayer. The lack of a transitional layer is therefore similar to that found on metal surfaces, which is in good accord with the semimetallic nature of the $\sqrt{3}\times\sqrt{3}$-Ag template. Our DFT calculations show that a bridge site provides the most stable adsorption site for cysteine when compared to the 3-fold hollow or atop site on a $\sqrt{3}\times\sqrt{3}$-Ag terrace surface. As the availability of other types of bridge sites is expected to be more prevalent at the step edges (and other defects), our DFT result is consistent with the observed initial growth first on step edges. The formation of a S-to-metal bond allows, at most, one additional functional group to be sufficiently close to enable interaction with a second surface atom (due to the inherent structure of cysteine itself), thus favoring the bridge site. This also leaves the remaining (third) functional group free to undergo further interaction with other incoming adspecies. At elevated temperatures, cysteine adspecies are found to transform the monatomic Ag layer of $\sqrt{3}\times\sqrt{3}$-Ag into Ag agglomerates of nanometer sizes by cleavage of Ag−Si bonds and formation of Ag−S and Si−NH bonds. This is an important result because cysteine-induced cluster formation at elevated temperature offers a new approach of using adsorbates to convert a two-dimensional, single-atom-thick $\sqrt{3}\times\sqrt{3}$-Ag overlayer to, in effect, zero-dimensional nanoclusters. The present work further highlights the possibility of taking advantage of the unique surface chemistry on this and similar intricate two-dimensional metal overlayers as templates to grow nanoclusters or quantum dots for chemical sensing and catalysis applications.

## ■ ASSOCIATED CONTENT

### Supporting Information

The Supporting Information is available free of charge on the ACS Publications website at DOI: 10.1021/acs.langmuir.9b02852.

Binding energies and relative peak areas of spectral features at different exposures and thermal treatment steps, time-sequence empty-state STM images for 30 s cysteine exposure, and detailed results of large-scale DFT calculations for the adsorption configurations of three cysteine conformers in single and dimer modes (PDF)

## ■ AUTHOR INFORMATION


### Corresponding Author

*E-mail: tong@uwaterloo.ca.

### ORCID

Fatemeh R. Rahsepar: 0000-0003-2359-2523

Kam Tong Leung: 0000-0002-1879-2806

### Present Address

†F.R.R.: School of Chemistry, College of Science, University of Tehran, Tehran, Iran.


### Notes

The authors declare no competing financial interest.

## ■ ACKNOWLEDGMENTS

This work was supported by the Natural Sciences and Engineering Research Council of Canada.

## ■ REFERENCES


(1) Le Lay, G.; Aristov, V. Y.; Seehofer, L.; Buslaps, T.; Johnson, R. L.; Gothelid, M.; Hammar, M.; Karlsson, U. O.; Flodstrom, S. A.; Feidenhans'l, R.; Nielsen, M.; Findeisen, E.; Uhrberg, R. I. G. STM and Synchrotron Radiation Studies of "Prototypical" Metal/Semiconductor Systems. *Surf. Sci.* **1994**, *307−309*, 280−294.

(2) Zhang, H. M.; Gustafsson, J. B.; Johansson, L. S. O. Surface Atomic Structure of Ag/Si-$\sqrt{3}\times\sqrt{3}$. *Phys. Rev. B: Condens. Matter Mater. Phys.* **2006**, *74*, 201304.

(3) Matsuda, I.; Morikawa, H.; Liu, C.; Ohuchi, S.; Hasegawa, S.; Okuda, T.; Kinoshita, T.; Ottaviani, C.; Cricenti, A.; D'angelo, M.; et al. Electronic Evidence of Asymmetry in the Si(111)$\sqrt{3}\times\sqrt{3}$-Ag Structure. *Phys. Rev. B: Condens. Matter Mater. Phys.* **2003**, *68*, 85407.

(4) Takahashi, T.; Nakatani, S.; Okamoto, N.; Ishikawa, T.; Kikuta, S. A Study of the Si (111)$\sqrt{3}\times\sqrt{3}$-Ag Surface by Transmission X-Ray Diffraction and X-Ray Diffraction Topography. *Surf. Sci. Lett.* **1991**, *242*, A35.

(5) Ding, Y. G.; Chan, C. T.; Ho, K. M. Structure of the ($\sqrt{3}\times\sqrt{3}$)R30°Ag/Si(111) Surface from First-Principles Calculations. *Phys. Rev. Lett.* **1991**, *67*, 1454.

(6) Takahashi, T.; Nakatani, S.; Okamoto, N.; Ishikawa, T.; Kikuta, S. Study on the Si(111)$\sqrt{3}\times\sqrt{3}$-Ag Surface Structure by X-Ray Diffraction. *Jpn. J. Appl. Phys.* **1988**, *27*, L753−L755.

(7) Sato, N.; Nagao, T.; Hasegawa, S. Si(111)-($\sqrt{3}\times\sqrt{3}$)-Ag Surface at Low Temperatures: Symmetry Breaking and Surface Twin Boundaries. *Surf. Sci.* **1999**, *442*, 65−73.

(8) Aizawa, H.; Tsukada, M.; Sato, N.; Hasegawa, S. Asymmetric Structure of the Si(111)-$\sqrt{3}\times\sqrt{3}$-Ag Surface. *Surf. Sci.* **1999**, *429*, L509−L514.

(9) Kirchner, E. J. J; Baerends, E. J; Velde, G; Vlieg, E. A Study on the Si (111)-$\sqrt{3}\times\sqrt{3}$-Ag System II. Interaction between Substrate and Adsorbate. *Surf. Sci.* **1995**, *330*, 113−125.

(10) Gustafsson, J. B.; Zhang, H. M.; Moons, E.; Johansson, L. S. O. Electron Spectroscopy Studies of PTCDA on Ag/Si(111)-$\sqrt{3}\times\sqrt{3}$. *Phys. Rev. B: Condens. Matter Mater. Phys.* **2007**, *75*, 155413.

(11) Emanuelsson, C.; Johansson, L. S. O.; Zhang, H. M. Photoelectron Spectroscopy Studies of PTCDI on Ag/Si(111)-$\sqrt{3}\times\sqrt{3}$. *J. Chem. Phys.* **2018**, *149*, 044702.

(12) Yokoyama, T.; Kawasaki, M.; Asari, T.; Ohno, S.; Tanaka, M.; Yoshimoto, Y. Adsorption and Self-Assembled Structures of Sexithiophene on the Si(111)-$\sqrt{3}\times\sqrt{3}$-Ag Surface. *J. Chem. Phys.* **2015**, *142*, 204701.

(13) Ohno, S.; Tanaka, H.; Tanaka, K.; Takahashi, K.; Tanaka, M. Electronic Structure of a-Sexithiophene Ultrathin Films Grown on Si(111)-$\sqrt{3}\times\sqrt{3}$-Ag. *Phys. Chem. Chem. Phys.* **2018**, *20*, 1114−1126.

(14) Liu, R.; Fu, C.; Perepichka, D. F.; Gallagher, M. C. Supramolecular Structures of Halogenated Oligothiophenes on the Si(111)-$\sqrt{3}\times\sqrt{3}$-Ag Surface. *Surf. Sci.* **2016**, *647*, 51−54.




DOI: 10.1021/acs.langmuir.9b02852
*Langmuir* 2019, 35, 16185−16200

(15) Upward, M. D.; Beton, P. H.; Moriarty, P. Adsorption of Cobalt Phthalocyanine on Ag Terminated Si(111). *Surf. Sci.* **1999**, *441*, 21−25.
(16) Beggan, J. P.; Krasnikov, S. A.; Sergeeva, N. N.; Senge, M. O.; Cafolla, A. A. Self-Assembly of Ni(II) Porphine Molecules on the Ag/Si(111)-($\sqrt{3}\times\sqrt{3}$)R30° Surface Studied by STM/STS and LEED. *J. Phys.: Condens. Matter* **2008**, *20*, 015003.
(17) Li, Q.; Yamazaki, S.; Eguchi, T.; Kim, H.; Kahng, S. J.; Jia, J. F.; Xue, Q. K.; Hasegawa, Y. Initial Adsorption and Kondo Resonance of 5,10,15,20-Tetrakis(4-bromophenyl)porphyrin-Co Molecules on Ag/Si(111) Surface Studied by Low-Temperature Scanning Tunneling Microscopy/Spectroscopy. *Jpn. J. Appl. Phys.* **2009**, *48*, 08JB01.
(18) Baris, B.; Jeannoutot, J.; Luzet, V.; Palmino, F.; Rochefort, A.; Chérioux, F. Noncovalent Bicomponent Self-Assemblies on a Silicon Surface. *ACS Nano* **2012**, *6*, 6905−6911.
(19) Guaino, P.; Cafolla, A. A.; McDonald, O.; Carty, D.; Sheerin, G.; Hughes, G. Scanning Tunnelling Spectroscopy of Low Pentacene Coverage on the Ag/Si(111)-($\sqrt{3}\times\sqrt{3}$) Surface. *J. Phys.: Condens. Matter* **2003**, *15*, S2693−S2698.
(20) Sheerin, G.; Cafolla, A. A. Self-Assembled Structures of Trimesic Acid on the Ag/Si(111)-($\sqrt{3}\times\sqrt{3}$)R30° Surface. *Surf. Sci.* **2005**, *577*, 211−219.
(21) Suzuki, T.; Lutz, T.; Payer, D.; Lin, N.; Tait, S. L.; Costantini, G.; Kern, K. Substrate Effect on Supramolecular Self-Assembly: From Semiconductors to Metals. *Phys. Chem. Chem. Phys.* **2009**, *11*, 6498−6504.
(22) Perdigão, L. M. A.; Staniec, P. A.; Champness, N. R.; Kelly, R. E. A.; Kantorovich, L. N.; Beton, P. H. Experimental and Theoretical Identification of Adenine Monolayers on Ag-Terminated Si(111). *Phys. Rev. B: Condens. Matter Mater. Phys.* **2006**, *73*, 195423.
(23) Tegenkamp, C.; Schmeidel, J.; Pfnür, H. Chemisorption of Ferrocene on Si(111)-Ag$\sqrt{3}$: Frustrated Conformational Flexibility. *Surf. Sci.* **2011**, *605*, 267−271.
(24) Wandlowski, T.; Lampner, D.; Lindsay, S. M. Structure and Stability of Cytosine Adlayers on Au(111): An in-Situ STM Study. *J. Electroanal. Chem.* **1996**, *404*, 215−226.
(25) Kawai, T.; Tanaka, H.; Nakagawa, T. Low Dimensional Self-Organization of DNA-Base Molecules on Cu(111) Surfaces. *Surf. Sci.* **1997**, *386*, 124−136.
(26) Furukawa, M.; Tanaka, H.; Kawai, T. Formation Mechanism of Low-Dimensional Superstructure of Adenine Molecules and Its Control by Chemical Modification: A Low-Temperature Scanning Tunneling Microscopy Study. *Surf. Sci.* **2000**, *445*, 1−10.
(27) Furukawa, M.; Tanaka, H.; Kawai, T. The Role of Dimer Formation in the Self-Assemblies of DNA Base Molecules on Cu(111) Surfaces: A Scanning Tunneling Microscope Study. *J. Chem. Phys.* **2001**, *115*, 3419−3423.
(28) Otero, R.; Lukas, M.; Kelly, R. E. A.; Xu, W.; Lægsgaard, E.; Stensgaard, I.; Kantorovich, L. N.; Besenbacher, F. Elementary Structural Motifs in a Random Network of Cytosine Adsorbed on a Gold(111) Surface. *Science* **2008**, *319*, 312−315.
(29) Xu, W.; Kelly, R. E. A.; Otero, R.; Schöck, M.; Lægsgaard, E.; Stensgaard, I.; Kantorovich, L. N.; Besenbacher, F. Probing the Hierarchy of Thymine-Thymine Interactions in Self-Assembled Structures by Manipulation with Scanning Tunneling Microscopy. *Small* **2007**, *3*, 2011−2014.
(30) Kelly, R. E. A.; Lukas, M.; Kantorovich, L. N.; Otero, R.; Xu, W.; Mura, M.; Lægsgaard, E.; Stensgaard, I.; Besenbacher, F. Understanding the Disorder of the DNA Base Cytosine on the Au(111) Surface. *J. Chem. Phys.* **2008**, *129*, 184707.
(31) Kelly, R. E. A.; Xu, W.; Lukas, M.; Otero, R.; Mura, M.; Lee, Y. J.; Lægsgaard, E.; Stensgaard, I.; Kantorovich, L. N.; Besenbacher, F. An Investigation into the Interactions between Self-Assembled Adenine Molecules and Au(111) Surface. *Small* **2008**, *4*, 1494−1500.
(32) Otero, R.; Xu, W.; Lukas, M.; Kelly, R. E. A.; Lægsgaard, E.; Stensgaard, I.; Kjems, J.; Kantorovich, L. N.; Besenbacher, F. Specificity of Watson-Crick Base Pairing on a Solid Surface Studied at the Atomic Scale. *Angew. Chem.* **2008**, *120*, 9819−9822.
(33) Bald, I.; Wang, Y.-g.; Dong, M.; Rosen, C. B.; Ravnsbaek, J. B.; Zhuang, G.-l.; Gothelf, K. V.; Wang, J.-g.; Besenbacher, F. Control of Self-Assembled 2D Nanostructures by Methylation of Guanine. *Small* **2011**, *7*, 939−949.
(34) Liu, L.; Xia, D.; Klausen, L. H.; Dong, M. The Self-Assembled Behavior of DNA Bases on the Interface. *Int. J. Mol. Sci.* **2014**, *15*, 1901−1914.
(35) Mateo Marti, E.; Methivier, Ch.; Pradier, C. M. (S)-Cysteine Chemisorption on Cu(110), from the Gas or Liquid Phase: An FT-RAIRS and XPS Study. *Langmuir* **2004**, *20*, 10223−10230.
(36) Thomsen, L.; Wharmby, M. T.; Riley, D. P.; Held, G.; Gladys, M. J. The Adsorption and Stability of Sulfur Containing Amino Acids on Cu{531}. *Surf. Sci.* **2009**, *603*, 1253−1261.
(37) Canepa, M.; Pelori, P.; Lavagnino, L.; Bisio, F.; Moroni, R.; Terreni, S.; Mattera, L. He* Interaction with Soft Matter Surfaces: Ultra Thin L-Cysteine Films. *Nucl. Instrum. Methods Phys. Res., Sect. B* **2007**, *256*, 324−327.
(38) Fischer, S.; Papageorgiou, A. C.; Marschall, M.; Reichert, J.; Diller, K.; Klappenberger, F.; Allegretti, F.; Nefedov, A.; Wöll, C.; Barth, J. V. L-Cysteine on Ag(111): A Combined STM and X-Ray Spectroscopy Study of Anchorage and Deprotonation. *J. Phys. Chem. C* **2012**, *116*, 20356−20362.
(39) Luque, N. B.; Vélez, P.; Pötting, K.; Santos, E. Ab Initio Studies of the Electronic Structure of L-Cysteine Adsorbed on Ag(111). *Langmuir* **2012**, *28*, 8084−8099.
(40) Santos, E.; Avalle, L. B.; Scurtu, R.; Jones, H. L-Cysteine Films on Ag(111) Investigated by Electrochemical and Nonlinear Optical Methods. *Chem. Phys.* **2007**, *342*, 236−244.
(41) Santos, E.; Avalle, L.; Pötting, K.; Vélez, P.; Jones, H. Experimental and Theoretical Studies of L-Cysteine Adsorbed at Ag(111) Electrodes. *Electrochim. Acta* **2008**, *53*, 6807−6817.
(42) Schillinger, R.; Šljivančanin, Ž.; Hammer, B.; Greber, T. Probing Enantioselectivity with X-Ray Photoelectron Spectroscopy and Density Functional Theory. *Phys. Rev. Lett.* **2007**, *98*, 136102.
(43) Kühnle, A.; Molina, L. M.; Linderoth, T. R.; Hammer, B.; Besenbacher, F. Growth of Unidirectional Molecular Rows of Cysteine on Au(110)-(1×2) Driven by Adsorbate-Induced Surface Rearrangements. *Phys. Rev. Lett.* **2004**, *93*, 86101.
(44) Canepa, M.; Lavagnino, L.; Pasquali, L.; Moroni, R.; Bisio, F.; De Renzi, V.; Terreni, S.; Mattera, L. Growth Dynamics of L-Cysteine SAMs on Single-Crystal Gold Surfaces: A Metastable Deexcitation Spectroscopy Study. *J. Phys.: Condens. Matter* **2009**, *21*, 264005.
(45) Cossaro, A.; Terreni, S.; Cavalleri, O.; Prato, M.; Cvetko, D.; Morgante, A.; Floreano, L.; Canepa, M. Electronic and Geometric Characterization of the L-Cysteine Paired-Row Phase on Au(110). *Langmuir* **2006**, *22*, 11193−11198.
(46) Gonella, G.; Terreni, S.; Cvetko, D.; Cossaro, A.; Mattera, L.; Cavalleri, O.; Rolandi, R.; Morgante, A.; Floreano, L.; Canepa, M. Ultrahigh Vacuum Deposition of L-Cysteine on Au(110) Studied by High-Resolution X-Ray Photoemission: From Early Stages of Adsorption to Molecular Organization. *J. Phys. Chem. B* **2005**, *109*, 18003−18009.
(47) Höffling, B.; Ortmann, F.; Hannewald, K.; Bechstedt, F. Single Cysteine Adsorption on Au(110): A First-Principles Study. *Phys. Rev. B: Condens. Matter Mater. Phys.* **2010**, *81*, 45407.
(48) Höffling, B.; Ortmann, F.; Hannewald, K.; Bechstedt, F. Interface with Organic Molecules: Cysteine on Au(110). *Phys. Status Solidi C* **2010**, *7*, 149−152.
(49) Kühnle, A.; Linderoth, T. R.; Schunack, M.; Besenbacher, F. L-Cysteine Adsorption Structures on Au(111) Investigated by Scanning Tunneling Microscopy under Ultrahigh Vacuum Conditions. *Langmuir* **2006**, *22*, 2156−2160.
(50) Kühnle, A.; Linderoth, T. R.; Besenbacher, F. Enantiospecific Adsorption of Cysteine at Chiral Kink Sites on Au(110)-(1×2). *J. Am. Chem. Soc.* **2006**, *128*, 1076−1077.
(51) Chapman, C. R. L.; Ting, E. C. M.; Kereszti, A.; Paci, I. Self-Assembly of Cysteine Dimers at the Gold Surface: A Computational Study of Competing Interactions. *J. Phys. Chem. C* **2013**, *117*, 19426−19435.


DOI: 10.1021/acs.langmuir.9b02852
*Langmuir* 2019, 35, 16185−16200

(52) Buimaga-Iarinca, L.; Morari, C. Effect of Conformational Symmetry upon the Formation of Cysteine Clusters on the Au(110)-(1×1) Surface: A First-Principles Study. *J. Phys. Chem. C* **2013**, *117*, 20351−20360.
(53) Di Felice, R.; Selloni, A.; Molinari, E. DFT Study of Cysteine Adsorption on Au(111). *J. Phys. Chem. B* **2003**, *107*, 1151−1156.
(54) Di Felice, R.; Selloni, A. Adsorption Modes of Cysteine on Au(111): Thiolate, Amino-Thiolate, Disulfide. *J. Chem. Phys.* **2004**, *120*, 4906−4914.
(55) Mateo-Martí, E.; Rogero, C.; Gonzalez, C.; Sobrado, J. M.; De Andrés, P. L.; Martin-Gago, J. A. Interplay between Fast Diffusion and Molecular Interaction in the Formation of Self-Assembled Nanostructures of S-Cysteine on Au(111). *Langmuir* **2010**, *26*, 4113−4118.
(56) Kühnle, A. Self-Assembly of Organic Molecules at Metal Surfaces. *Curr. Opin. Colloid Interface Sci.* **2009**, *14*, 157−168.
(57) Kühnle, A.; Linderoth, T. R.; Hammer, B.; Besenbacher, F. Chiral Recognition in Dimerization of Adsorbed Cysteine Observed by Scanning Tunnelling Microscopy. *Nature* **2002**, *415*, 891−893.
(58) Fajín, J. L. C.; Gomes, J. R. B.; Cordeiro, M. N. D. S. DFT Study of the Adsorption of D-(L-)Cysteine on Flat and Chiral Stepped Gold Surfaces. *Langmuir* **2013**, *29*, 8856−8864.
(59) Rahsepar, F. R.; Zhang, L.; Farkhondeh, H.; Leung, K. T. Biofunctionalization of Si(111)7×7 by "Renewable" L-Cysteine Transitional Layer. *J. Am. Chem. Soc.* **2014**, *136*, 16909−16918.
(60) Wan, K. J.; Lin, X. F.; Nogami, J. Surface Reconstructions in the Ag/Si(111) System. *Phys. Rev. B: Condens. Matter Mater. Phys.* **1993**, *47*, 13700−13712.
(61) Wallace, W. E. Mass spectra; https://webbook.nist.gov/cgi/cbook.cgi?ID=C52904&Mask=200.
(62) Dobrowolski, J. C.; Rode, J. E.; Sadlej, J. Cysteine Conformations Revisited. *J. Mol. Struct. (Theochem)* **2007**, *810*, 129−134.
(63) Bensebaa, F.; Zhou, Y.; Deslandes, Y.; Kruus, E.; Ellis, T. H. XPS Study of Metal-Sulfur Bonds in Metal-Alkanethiolate Materials. *Surf. Sci.* **1998**, *405*, 472−476.
(64) Briggs, D. D.; Seah, M. P. *Practical Surface Analysis*, 2nd ed.; Wiley: Chichester, 1948.
(65) Dodero, G.; De Michieli, L.; Cavalleri, O.; Rolandi, R.; Oliveri, L.; Daccà, A.; Parodi, R. L-Cysteine Chemisorption on Gold: An XPS and STM Study. *Colloids Surf. A* **2000**, *175*, 121−128.
(66) Cavalleri, O.; Gonella, G.; Terreni, S.; Vignolo, M.; Floreano, L.; Morgante, A.; Canepa, M.; Rolandi, R. High Resolution X-Ray Photoelectron Spectroscopy of L-Cysteine Self-Assembled Film. *Phys. Chem. Chem. Phys.* **2004**, *6*, 4042−4046.
(67) Uvdal, K.; Bodö, P.; Liedberg, B. L-Cysteine Adsorbed on Gold and Copper: An X-Ray Photoelectron Spectroscopy Study. *J. Colloid Interface Sci.* **1992**, *149*, 162−173.
(68) Rahsepar, F. R.; Moghimi, N.; Leung, K. T. Surface-Mediated Hydrogen Bonding of Proteinogenic α-Amino Acids on Silicon. *Acc. Chem. Res.* **2016**, *49*, 942−951.
(69) Weiss, I. M.; Muth, C.; Drumm, R.; Kirchner, H. O. K. Thermal Decomposition of the Amino Acids Glycine, Cysteine, Aspartic Acid, Asparagine, Glutamic Acid, Glutamine, Arginine and Histidine. *BMC Biophys.* **2018**, *11*, 1−15.
(70) Stöhr, J.; Gland, J. L.; Kollin, E. B.; Koestner, R. J.; Johnson, A. L.; Muetterties, E. L.; Sette, F. Desulfurization and Structural Transformation of Thiophene on the Pt(111) Surface. *Phys. Rev. Lett.* **1984**, *53*, 2161−2164.
(71) Qiao, M. H.; Cao, Y.; Tao, F.; Liu, Q.; Deng, J. F.; Xu, G. Q. Electronic and Vibrational Properties of Thiophene on Si(100). *J. Phys. Chem. B* **2000**, *104*, 11211−11219.
(72) Kaushik, V. K. XPS Core Level Spectra and Auger Parameters for Some Silver Compounds. *J. Electron Spectrosc. Relat. Phenom.* **1991**, *56*, 273−277.
(73) Bensebaa, F.; Zhou, Y.; Deslandes, Y.; Kruus, E.; Ellis, T. H. XPS Study of Metal-Sulfur Bonds in Metal-Alkanethiolate Materials. *Surf. Sci.* **1998**, *405*, L472−L476.
(74) Powell, C. J. Elemental Binding Energies for X-Ray Photoelectron Spectroscopy. *Appl. Surf. Sci.* **1995**, *89*, 141−149.
(75) Oura, K.; Sumitomo, K.; Kobayashi, T.; Kinoshita, T.; Tanaka, Y.; Shoji, F.; Katayama, I. Adsorption of H on Si(111)-$\sqrt{3}\times\sqrt{3}$-Ag: Evidence for Ag(111) Agglomerates Formation. *Surf. Sci.* **1991**, *254*, L460−L464.
(76) Shibata, A.; Kimura, Y.; Takayanagi, K. On the Restructured Layer of the Si(111)$\sqrt{3}\times\sqrt{3}$-Ag Structure Studied by Scanning Tunneling Microscopy. *Surf. Sci.* **1992**, *275*, L697−L701.
(77) Shibata, A.; Takayanagi, K. Restructuring of the Reconstructed Si(111)7×7 Surface by Metal (Au, Ag) Deposition. *Jpn. J. Appl. Phys.* **1993**, *32*, 1385−1388.
(78) Watanabe, S.; Aono, M.; Tsukada, M. Theoretical Calculations of the Scanning-Tunneling-Microscopy Images of the Si(111)$\sqrt{3}\times\sqrt{3}$-Ag Surface. *Phys. Rev. B: Condens. Matter Mater. Phys.* **1991**, *44*, 8330−8333.
(79) Belianinov, A. A.; Ünal, B.; Lu, N.; Ji, M.; Ho, K. M.; Wang, C. Z.; Tringides, M. C.; Thiel, P. A. Islands and Holes as Measures of Mass Balance in Growth of the $(\sqrt{3}\times\sqrt{3})$R30° Phase of Ag on Si(111). *Phys. Rev. B: Condens. Matter Mater. Phys.* **2010**, *82*, 165429.
(80) McComb, D. W.; Wolkow, R. A.; Hackett, P. A. Defects on the Ag/Si(111)-$(\sqrt{3}\times\sqrt{3})$ Surface. *Phys. Rev. B: Condens. Matter Mater. Phys.* **1994**, *50*, 18268−18274.
(81) Venable, J. A. *Introduction to Surface and Thin Film Processes*; Cambridge University Press: Cambridge, 2003.
(82) Barth, J. V.; Costantini, G.; Kern, K. Engineering Atomic and Molecular Nanostructures at Surfaces. *Nature* **2005**, *437*, 671−679.
(83) Oura, K.; Ohnishi, H.; Yamamoto, Y.; Katayama, I.; Ohba, Y. Atomic-Hydrogen-Induced Ag Cluster Formation on Si(111)-$\sqrt{3}\times\sqrt{3}$-Ag Surface Observed by Scanning Tunneling Microscopy. *J. Vac. Sci. Technol. B: Microelectron. Process. Phenom.* **1996**, *14*, 988−991.
(84) Williams, B. R.; Mason, B. F.; McComb, D. W.; Moffatt, D. J.; Hackett, P. A. A Scanning Tunneling Microscopy Investigation of the Reaction of Hydrogen Atoms with Ag/Si(111)-$(\sqrt{3}\times\sqrt{3})$. *Surf. Sci.* **1994**, *313*, L790−L796.
(85) Ohnishi, H.; Yamamoto, Y.; Katayama, I.; Ohba, Y.; Oura, K. Hydrogen-Induced Ag Cluster Formation on the Si(111)$\sqrt{3}\times\sqrt{3}$-(R30°)-Ag Surface Observed by Scanning Tunneling Microscopy. *Jpn. J. Appl. Phys.* **1994**, *33*, L1106−L1109.
(86) Li, B. Q.; Zuo, J. M. Self-Assembly of Epitaxial Ag Nanoclusters on H-Terminated Si(111) Surfaces. *J. Appl. Phys.* **2003**, *94*, 743−748.
(87) Gronert, S.; O'Hair, R. A. J. Ab Initio Studies of Amino Acid Conformations. 1. The Conformers of Alanine, Serine, and Cysteine. *J. Am. Chem. Soc.* **1995**, *117*, 2071−2081.
(88) Cottrell, T. L. *The Strengths of Chemical Bonds*, 2nd ed.; Butterworths Scientific Publications: London, 1958.
(89) Luo, Y. R. *Comprehensive Handbook of Chemical Bond Energies*; CRC Press: Boca Raton, 2007.


DOI: 10.1021/acs.langmuir.9b02852
*Langmuir* 2019, 35, 16185−16200